iScience

Article

Elevated labile iron contributes to membrane repair deficits in facioscapulohumeral muscular dystrophy

Graphical abstract

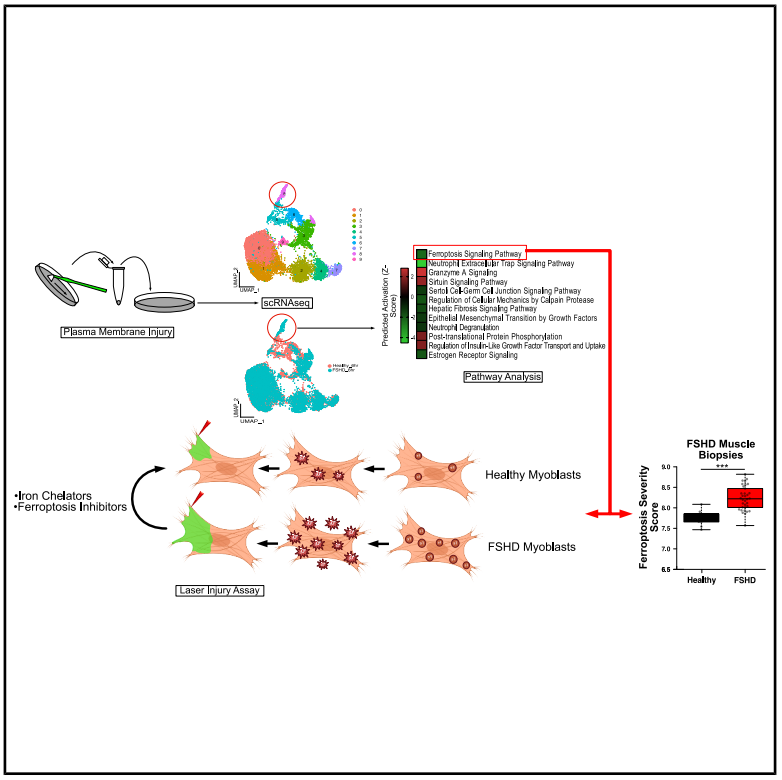

Highlights

- Plasma membrane (PM) injury stimulates DUX4 expression in FSHD myoblasts
- FSHD myoblasts and muscle tissue demonstrate signs of ferroptotic stress
- Increasing labile iron worsens PM repair in FSHD but not healthy myoblasts
- Iron chelation and ferroptosis inhibition improve PM repair in FSHD myoblasts

Authors

Adam J. Bittel, Surajit Bhattacharya, Lulya Okubamariam, Yi-Wen Chen

Correspondence

abittel@childrensnational.org (A.J.B.), ychen@childrensnational.org (Y.-W.C.)

In brief

Biological sciences

Bittel et al., 2026, iScience *29*, 115781
June 19, 2026
https://doi.org/10.1016/j.isci.2026.115781

CellPress

iScience

CellPress
OPEN ACCESS

Article

Elevated labile iron contributes to membrane repair deficits in facioscapulohumeral muscular dystrophy

Adam J. Bittel,[1,*] Surajit Bhattacharya,[1] Lulya Okubamariam,[1] and Yi-Wen Chen[1,2,3,*]
[1]Center for Genetic Medicine Research, Children's National Research and Innovation Campus, Washington, DC 20012, USA
[2]Department of Genomics and Precision Medicine, Department of Pediatrics, Department of Biochemistry and Molecular Medicine, School of Medicine and Health Science, The George Washington University, Washington, DC 20037, USA
[3]Lead contact
*Correspondence: abittel@childrensnational.org (A.J.B.), ychen@childrensnational.org (Y.-W.C.)
https://doi.org/10.1016/j.isci.2026.115781

SUMMARY

Facioscapulohumeral muscular dystrophy (FSHD) is caused by expression of the transcription factor DUX4, which is associated with plasma membrane (PM) repair deficits. Here, we show that PM injury triggers a mild but significant increase in DUX4 mRNA expression in FSHD myoblasts. These cells demonstrate the dysregulation of genes critical for PM repair, which are sensitive and specific for FSHD muscle tissue, and include regulators of ferroptosis. FSHD myoblasts also present with elevated labile ferrous iron and lipid peroxidation—hallmarks of ferroptotic stress. In FSHD muscle biopsies, the expression of ferroptosis biomarkers is elevated, predictive of inflammation. and positively correlated with fatty infiltration. Increasing labile iron and lipid peroxidation worsen PM repair in FSHD myoblasts, while treatment with the iron chelator 2,2′-Bipyridyl and ferroptosis inhibitor ferrostatin-1 improves repair. These data are the first to identify signs of ferroptotic stress in human FSHD myoblasts and demonstrate the potential benefit of targeting ferroptosis in FSHD.

INTRODUCTION

Facioscapulohumeral muscular dystrophy (FSHD) is an autosomal dominant muscular dystrophy that affects 1 in 7500 worldwide.[1,2] FSHD typically develops during the teen years in the facial and scapulohumeral muscles and progresses distally over time, making activities of daily living more challenging.[2] The disease is subcategorized into two types: FSHD1 and FSHD2. FSHD1 is caused by the loss of D4Z4 repeats in chromosome 4q35 in the presence of a permissive 4qA haplotype, leading to stable transcription of the double homeobox protein 4 (DUX4) transcription factor.[3–6] FSHD2 is linked to mutations in chromatin modifiers of the D4Z4 repeat array, including structural maintenance of chromosomes flexible hinge domain containing 1 (*SMCHD1*), DNA methyltransferase 3 beta (*DNMT3B*), and ligand-dependent nuclear receptor interacting factor 1 (*LRIF1*) genes in the presence of the 4qA haplotype, leading to hypomethylation of the D4Z4 region and DUX4 transcription.[7–9]

Aberrant expression of double homeobox protein 4 (*DUX4*) has been proposed to cause FSHD by activating a series of epigenetic and transcriptomic abnormalities in skeletal muscle and muscle-derived myoblasts.[10–12] DUX4 interferes with the expression of key genes involved in the myogenic program, disrupts oxidative stress responses and mitochondrial function, and is implicated in the onset of inflammation and fibrosis commonly found in patient skeletal muscle biopsies.[13–15] While the factors triggering DUX4 expression are poorly understood, cellular stress, including signals from oxidative stress, DNA damage, and differentiation, has all been implicated.[16–18] However, DUX4 target gene expression has been identified as a weak biomarker of FSHD status, with several molecular mechanisms of this disease hypothesized to occur as a downstream response to DUX4-mediated network rewiring.[19] These ancillary mechanisms, and their associated transcriptional changes, may be leveraged to identify features of FSHD cells and tissues.

Plasma membrane (PM) injury is a type of repetitive and routine cell stress in skeletal muscle that develops from daily physical activity as force is transmitted between the extracellular matrix and the cytoskeleton during muscle contraction.[20] These insults to the sarcolemma need to be repaired quickly (reviewed in[21]) to maintain cell integrity, and failure to appropriately repair membrane damage contributes to cell death and degeneration. We recently demonstrated that human FSHD myoblasts and mature skeletal muscle from a mouse model of FSHD (*FLEx-DUX4*) also display impaired sarcolemmal repair capacity, which could be improved through DUX4 knockdown and treatment with the antioxidant Trolox.[22] Poor membrane repair can lead to chronic activation of calcium, ROS, and metabolite signaling, which has been shown to induce stress, alter the cell epigenome, and elicit unfavorable transcriptional reprogramming in multiple diseases.[23] These transcriptional changes may also be used to identify gene signatures of FSHD skeletal muscles, which often display signs of myofiber degeneration and regeneration correlating with disease severity.[24]

DUX4 expression was reported to induce cell death *in vitro* and *in vivo*[25–27] via apoptosis and necroptosis pathways.[28,29] Our lab, and others, have identified oxidative stress and reactive oxygen species (ROS) damage as a major mechanism of DUX4 toxicity.[22,30] However, there are many sources of ROS, and multiple forms of oxidative cell death, including ferroptosis, pyroptosis, paraptosis, parthanatos, and oxeiptosis.[31] Additionally, while previous studies have implicated deficiencies in electron transport chain (ETC) complex I function as a major source of ROS in response to DUX4 expression, our lab also published evidence for elevated mitochondrial iron in FSHD immortalized human myoblasts.[32,33] Iron is an essential cofactor in iron-sulfur cluster-containing proteins, heme-containing proteins, and iron-ion-containing proteins of the ETC.[34] However, excessive elevation of mitochondrial iron can provide surplus substrate for the Fenton reaction—a process that generates hydroxyl radicals and subsequent lipid peroxidation, membrane damage, and activation of Ferroptosis.[35] Indeed, Nakamura et al. (2025) presented evidence for abnormal iron accumulation in FSHD muscle biopsies and a mouse model of FSHD, and that DUX4 leads to the activation of ferroptosis pathways.[36] Further investigation is needed to determine the regulation and activation of ferroptosis in FSHD cells and tissues, and if membrane damage contributes to this process.

Therefore, we aimed to elucidate the role of PM injury on DUX4 expression and the myocyte transcriptome at the single-cell level to better understand the cellular implications of membrane injury in FSHD. We hypothesized that PM injury stimulates DUX4 expression, and promotes cellular stress and unfavorable transcriptional changes that may contribute to disease onset or progression.

RESULTS

Plasma membrane injury triggers cell death and DUX4 expression in FSHD myoblasts

To investigate transcriptional response to PM injury, we utilized a bulk cell scrape approach (Figure 1A), which injures 96–99% of cells, from which ≥75% recover (Figures 1B–1D). Similar to our previous findings,[22] a significantly greater percentage of FSHD myoblasts fail to repair following scrape-injury (Figure 1D, $p < 0.05$). Assessment of *DUX4* mRNA expression at baseline, 6-, and 24-h post-injury indicated PM injury triggers a significant increase in *DUX4* expression by 6-h post-injury, which remained elevated through 24-h (Figure 1E, $p < 0.05$). However, the level of DUX4 expression was significantly less than that observed during FSHD myoblast differentiation into myotubes ($p < 0.001$, Figure 1E), which is commonly used to study *DUX4* expression *in vitro*.[26,37]

Single-cell RNAseq identifies FSHD gene signatures associated with low levels of DUX4 expression from PM injury

To characterize the transcriptional response to injury, we utilized single-cell RNA sequencing (scRNAseq) of two pairs of FSHD and healthy sibling donor myoblasts at baseline, and 6-h post-PM injury. scRNAseq failed to identify any cells expressing *DUX4*, or commonly reported *DUX4* downstream targets *ZSCAN4, TRIM43, MBD3L2, LEUTX, PRAMEF1, KHDC1L, RFPL2*, or *DUX4* pseudogenes *DUXA* and *DUXB* at either timepoint. These findings coincide with previous single-cell and single-nucleus RNA sequencing studies in FSHD, which also struggled to identify cells/nuclei expressing DUX4, even in differentiated myotubes.[38–40] Therefore, to further confirm our *DUX4* expression results, we used qRT-PCR to quantify the expression of *DUX4* downstream targets *MBD3L2* and *ZSCAN4* at baseline, 6-, and 24-h post-injury. We observed significant increases in *MDB3L2* expression at 6-h post-injury, which remained elevated through 24-h, and was also significantly lower than *MBD3L2* expression in FSHD myotubes ($p < 0.5$, Figure 1F). While we observed increases in *ZSCAN4* expression at 6-h post-injury, the increase did not reach significance relative to uninjured FSHD or healthy myoblasts at any timepoint (Figure 1G). The level of injury-induced *ZSCAN4* expression was also lower than in differentiated FSHD myotubes ($p < 0.001$, Figure 1G).

Given the low expression of DUX4 identified in this study, we used a pseudobulk analysis to define genes that differentiate FSHD from healthy myoblasts. From 196 common differentially expressed (DE) genes between FSHD and healthy myoblast at baseline, 125 were DE in the same direction (47 upregulated, 78 downregulated) (Figures 2A and 2B). The 47 upregulated genes formed our baseline gene signature (Figure 2B and Table S3), which was significantly elevated in FSHD myoblasts at baseline and 6-h post-injury in both donor pairs (all $p < 0.001$) (Figure 2C), and showed enrichment/predicted activation of pathways related to protein translation elongation and initiation, ribosomal RNA processing, nonsense mediated decay, and stress response signaling, and enrichment/downregulation of mitochondrial RNA and tRNA processing, cell cycle processes, degradation of the extracellular matrix, and MHC class II antigen presentation (Figure 2G and Table S4). Likewise, from 171 common DE genes between FSHD and healthy myoblasts at 6-h, 102 were DE in the same direction (48 upregulated, 54 downregulated) (Figures 2D and 2E, and Table S5). The 48 upregulated genes formed our 6-h gene signature, which was significantly elevated in FSHD myoblasts at baseline and 6-h post-injury in both donor pairs (all $p < 0.001$) (Figure 2F), and showed enrichment/predicted activation of connective tissue deposition pathways, cell adhesion pathways, granzyme A signaling, and degradation of the extracellular matrix pathways, and enrichment/predicted downregulation of ETC function and ATP synthesis pathways (Figure 2H and Table S6).

Single-cell RNAseq-derived FSHD gene signatures are predictive of disease status in FSHD human muscle biopsies

To validate our baseline and 6-h gene signatures *in vivo*, we retrieved the average expression of these genes in FSHD vs. healthy human muscle biopsies profiled in the studies by Yao et al. (2014),[41] Rahimov et al. (2012),[42] Dixit et al. (2007),[3] Wang et al. (2019),[15] Osborne et al. (2007),[43] and Tasca et al. (2012).[44] We then pooled the differences in expression across studies using an inverse variance, random effects meta-analysis. Our baseline gene signature was significantly elevated in FSHD biopsies in four of six studies (Mann-Whitney U test $p < 0.05$), with a significant pooled

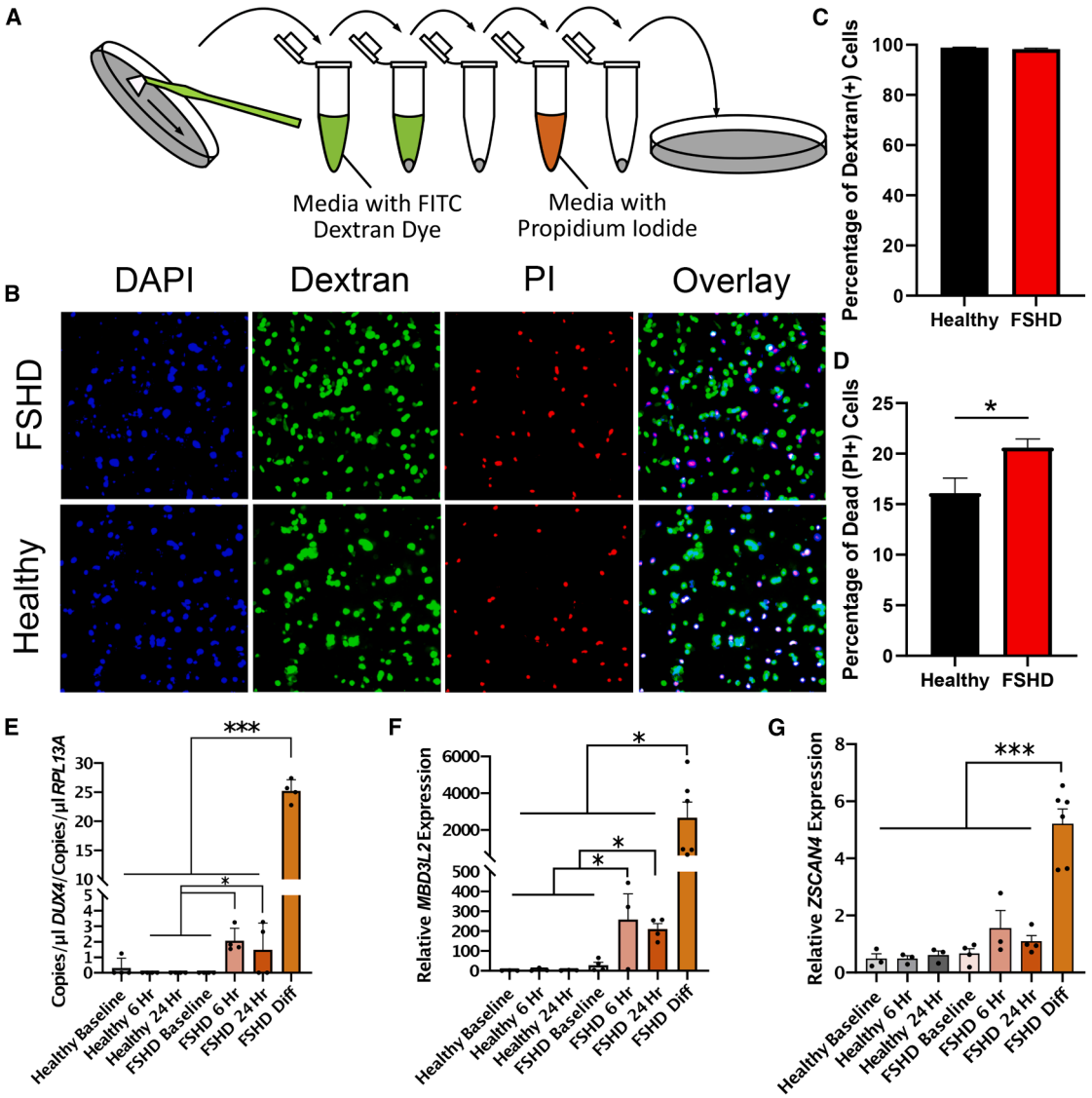

Figure 1. Plasma membrane injury triggers DUX4 expression in FSHD myoblasts

(A) Depiction of the cell scrape approach in which cells are mechanically scraped from the culture dish to induce membrane injury. Uptake of membrane-impermeable FITC dextran dye is used to identify injured cells. Propidium iodide (PI) is used to identify cells that fail to repair.

(B) Sample images of dextran (green) and PI (red) labeled FSHD and healthy myoblasts after PM injury, with DAPI to label nuclei.

(C) Quantification of the percentage of dextran(+) cells after injury.

(D) Percentage of healthy and FSHD myoblasts that fail to repair (% that are PI(+)). * denotes $p < 0.05$. $n = 7$ independent repeat experiments with FSHD Donor 2 cell lines and $n = 6$ independent repeat experiments with healthy donor 2 myoblasts.

(E) Copies/ul of *DUX4* mRNA in healthy ($n = 4$ cell lines) and FSHD myoblasts ($n = 4$ cell lines) at baseline, 6-h, and 24-h post-injury, as well as in differentiated FSHD myotubes ($n = 4$) normalized to copies/ul of *RPL13A*. * denotes $p < 0.05$ and *** denotes $p < 0.001$.

(F) Relative *MBD3L2* expression in healthy ($n = 3$) and FSHD myoblasts (n = 3–4 cell lines) at baseline, 6-h, and 24-h post-injury, as well as in differentiated FSHD myotubes ($n = 4$ cell lines, with 2 additional independent repeat experiments with cells from donors 1 and 2). * denotes $p < 0.05$.

(G) Relative *ZSCAN4* expression in healthy ($n = 4$ cell lines) and FSHD myoblasts ($n = 4$ cell lines) at baseline, 6-h, and 24-h post-injury, as well as in differentiated FSHD myotubes ($n = 4$ cell lines, with 2 independent repeat experiments with cells from donors 1 and 2). *** denotes $p < 0.001$. All values are mean ± SEM.

standard mean difference in expression (log normalized counts) of 1.14 (0.31–1.96) (Z = 2.70, $p = 0.007$) (Figure 3A). Likewise, our 6-h gene signature was significantly elevated in five of six studies (Mann-Whitney U test $p < 0.05$), with a significant pooled standard mean difference of 1.13 (0.75–1.51) (Z = 5.83, $p < 0.001$) (Figure 3B). To further validate the predictive ability of these genes, we used a receiver operator approach as outlined in Banerji et al. (2017).[19] We found that our baseline signature was a significant classifier of FSHD status in five of six studies (AUC of all ROC curves $p < 0.05$ except baseline signature in Rahimov et al. (2012),[42] and 6 h signature in Dixit et al. (2007)[3])

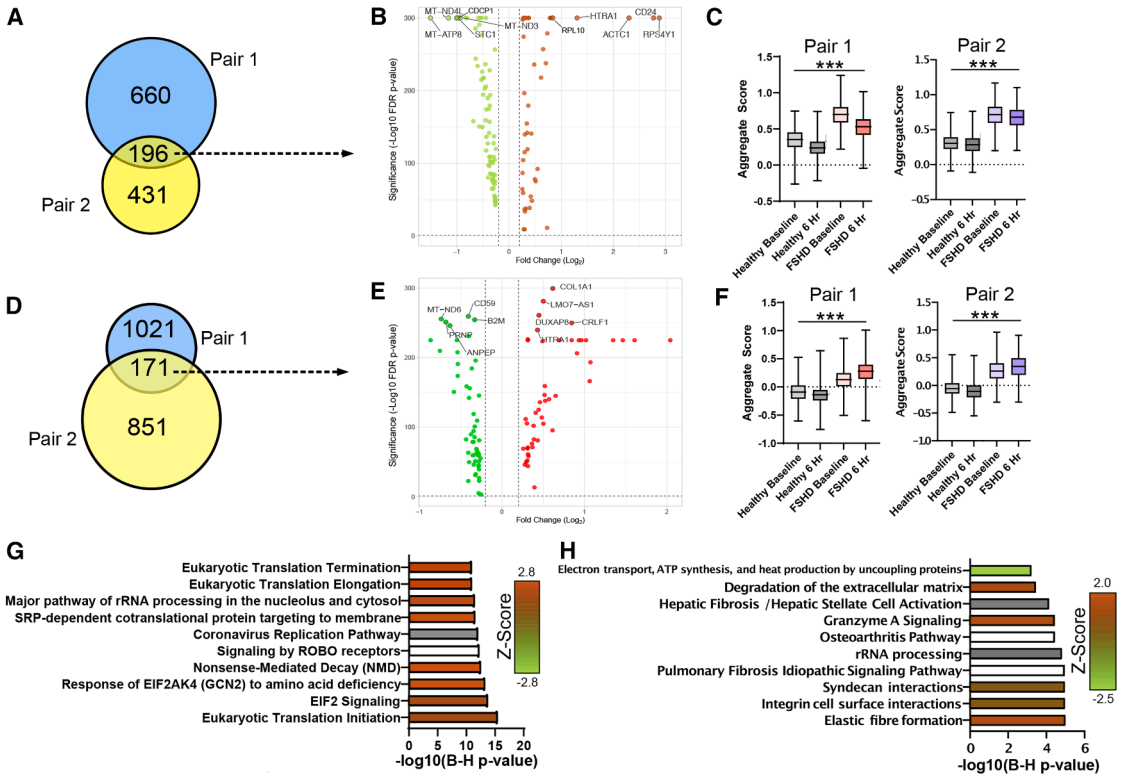

Figure 2. FSHD gene signatures associated with low levels of DUX4 expression

(A) Venn diagram shows the number of differentially expressed (DE) genes between healthy 1 and FSHD 1 donor myoblasts, and healthy 2 and FSHD 2 donors, and the number of DE genes they share in common.

(B) Volcano plot shows the log2Fold change and -log10(FDR *p*-value) of common upregulated (red) and downregulated (green) genes in both pairs at baseline. The top 10 upregulated/downregulated genes are labeled.

(C) Module score for our baseline gene signature in donor pairs 1 and 2. two-Way ANOVA: significant interaction between genotype (FSHD, healthy) and time (baseline, 6-h, 24-h) $p < 0.001$. Post-hoc testing: all groups significantly different $p < 0.001$.

(D–F) As in A-D but in healthy and FSHD samples collected at 6-h post-injury.

(G) The top 12 IPA-enriched pathways in the baseline gene signature (FDR *p*-value of <0.05). Bars are colored according to their predicted activation *Z* score (green = downregulated, red = upregulated, gray = no predicted *Z* score).

(H) The top 12 IPA-enriched pathways from 6-h gene signature (FDR *p* value of <0.05). Bars are colored according to their predicted activation *Z* score (green tones = downregulated pathways, red tones = upregulated pathways, gray = no predicted *Z* score).

(Figures 3C–3H and Table S7). Likewise, our 6-h gene signature was a significant classifier of FSHD status in five of six studies (all $p < 0.05$, Figures 3C–3H and Table S7).

To further validate the performance of our signatures, we benchmarked them against established transcriptional biomarker gene sets published by Banerji et al. (2017)[19] (pax7 target gene repression), Geng et al. (2012),[45] Choi et al. (2016),[46] and Yao et al. (2014).[41] We found significant overlap in the ROC curves of all 6 gene sets (our baseline and 6-h signatures and four biomarker gene sets, all AUC >0.90), and all six were equally effective at classifying FSHD and healthy muscle biopsies from the study by Wang et al. (2019)[15] (all DeLong comparisons $p > 0.05$). Furthermore, the expression of our baseline and 6-h signatures were significantly elevated with increasing histopathologic signs of disease severity ($p < 0.05$ for baseline and 6-h signatures, Figures S1E and S1F), and positively correlated with the expression of DUX4 candidate biomarkers *PRAMEF2, TRIM43*, and *KHDC1L* (baseline signature: r = 0.547, $p = 0.0008$, 6-h signature: r = 0.6155, $p < 0.001$, Figures S1G and S1H).

Both gene signatures share 18 genes in common, including *CD24, KRT81, HAS1, MFAP5, ACTC1, TNNT1, UCHL1, IGFBP4, CRLF1, IGFBP7, ALDH1A1, ENAH, LMO7-AS1, ADAMTS5, SULF1, HTRA1, PDLIM3,* and *SERF2.* These genes alone were significant classifiers of FSHD status, and were significantly elevated in muscle biopsies from all studies except those collected by Dixit et al. (2007) (all Mann-Whitney U $p < 0.05$). However, there was no significant difference in the performance of these genes compared to our baseline and 6-h gene signatures (all DeLong Tests $p > 0.05$).

Unique transcriptional responses to PM injury in FSHD myoblasts

IPA analysis of DE genes between FSHD and healthy myoblasts in each sibling pair at 6-h (Figure 2D) identified dysregulation of ferroptosis signaling, as well as neutrophil extracellular trap,

A Baseline Gene Signature

Study or Subgroup	FSHD Mean	FSHD SD	FSHD Total	Healthy Mean	Healthy SD	Healthy Total	Weight	Std. Mean Difference IV, Random, 95% CI	
Dixit et al. (2007)	10.24	0.21	14	9.94	0.2	6	15.4%	1.39 [0.32, 2.46]	**
Osborne et al. (2007)	9.27	0.2	19	9.08	0.12	30	18.6%	1.20 [0.58, 1.83]	**
Rahimov et al. (2012)	8.73	0.12	26	8.77	0.07	24	19.0%	-0.40 [-0.96, 0.16]	
Tasca et al. (2012)	10.34	0.18	8	10.01	0.09	7	13.4%	2.13 [0.78, 3.48]	**
Wang et al. (2019)	10.84	0.33	34	10.26	0.3	9	17.2%	1.76 [0.92, 2.59]	***
Yao et al. (2014)	11.55	0.19	15	11.35	0.1	8	16.4%	1.16 [0.23, 2.10]	
Total (95% CI)			**116**			**84**	**100.0%**	**1.14 [0.32, 1.96]**	

Heterogeneity: Tau² = 0.85; Chi² = 29.62, df = 5 (P < 0.0001); I² = 83%
Test for overall effect: Z = 2.72 (P = 0.007)

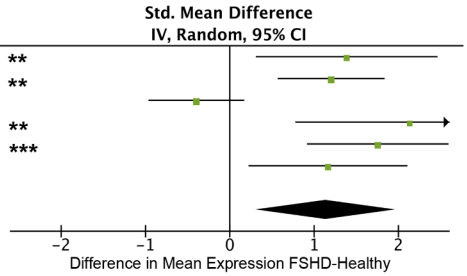

B 6 HR Gene Signature

Study or Subgroup	FSHD Mean	FSHD SD	FSHD Total	Healthy Mean	Healthy SD	Healthy Total	Weight	Std. Mean Difference IV, Random, 95% CI	
Dixit et al. (2007)	10.13	0.21	14	9.78	0.44	6	11.1%	1.15 [0.11, 2.18]	
Osborne et al. (2007)	7.6	0.29	19	7.35	0.1	30	23.7%	1.26 [0.63, 1.89]	***
Rahimov et al. (2012)	8.66	0.14	26	8.57	0.17	24	27.2%	0.57 [0.00, 1.14]	*
Tasca et al. (2012)	9.28	0.28	8	8.93	0.05	7	8.5%	1.58 [0.37, 2.79]	*
Wang et al. (2019)	10.54	0.39	34	9.89	0.25	9	15.9%	1.74 [0.91, 2.57]	***
Yao et al. (2014)	11.35	0.26	15	11.12	0.11	8	13.6%	1.00 [0.09, 1.92]	*
Total (95% CI)			**116**			**84**	**100.0%**	**1.13 [0.75, 1.50]**	

Heterogeneity: Tau² = 0.05; Chi² = 6.52, df = 5 (P = 0.26); I² = 23%
Test for overall effect: Z = 5.89 (P < 0.00001)

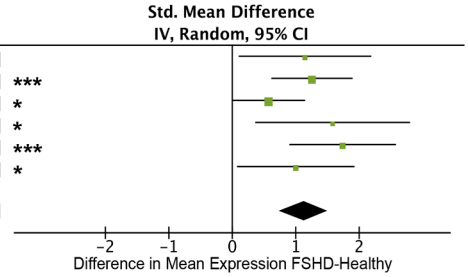

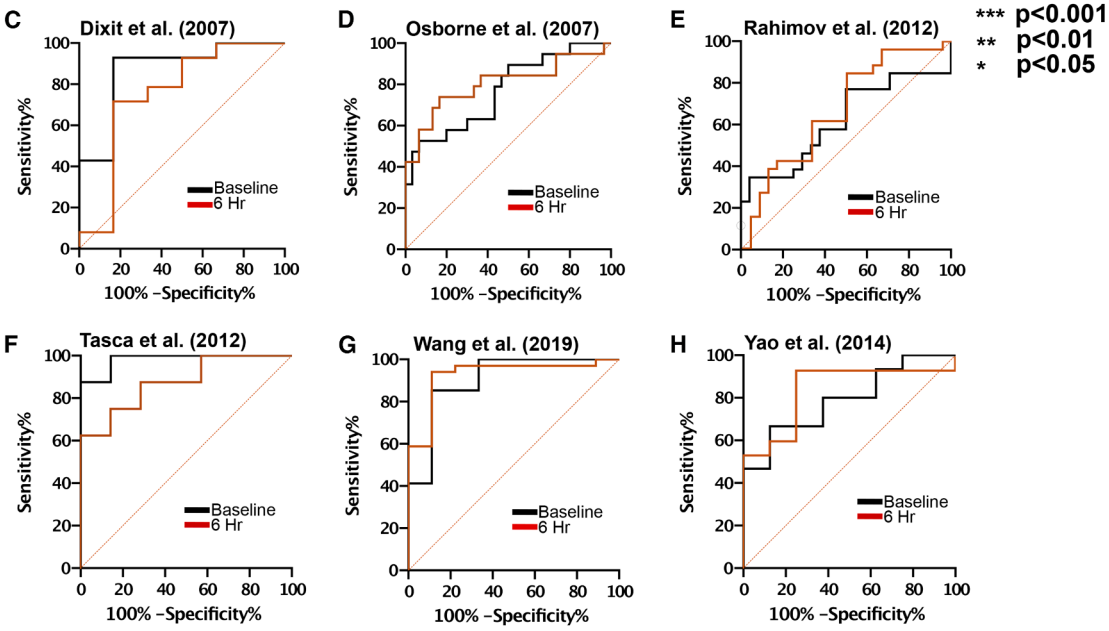

Figure 3. Validity and predictive power of single-cell RNAseq-derived FSHD gene signatures

(A) Results of an inverse variance weighted, random effects meta-analysis of the standardized mean difference in the average expression of our baseline scRNAseq-derived FSHD gene signature in FSHD vs. healthy human muscle biopsies. For each study, the average and standard deviation (SD) normalized expression of the genes in the signature is listed for FSHD and healthy biopsies. The weight given to each study in the meta-analysis is also listed, as well as the standard mean difference in expression for each study. The forest plot depicts the standard mean difference (location of green box), the weight (size of the green box), and 95% confidence interval (CI) of the difference (whiskers) for each study, as well as the pooled standard mean difference (black diamond denoting pooled estimate and 95% CI). A standardized mean difference <0 indicates expression is higher in healthy muscle biopsies, while >0 indicates expression is lower in healthy muscle biopsies. * denotes significant difference in average expression FSHD vs. healthy (Mann-Whitney U test, *$p < 0.05$, **$p < 0.01$, and ***$p < 0.001$) in each individual study.

(B) Same as in A, but for our 6-h gene signature.

(C) ROC curve compares the discriminatory power of our baseline (black line) and 6-h (light red line) gene signatures in the microarray data collected by Dixit et al. (2007).[3]

(D) As in C, but in the microarray study conducted by Osborne et al. (2007).[43]

(E) As in C, but in the microarray study conducted by Rahimov et al. (2012).[42]

(F) As in C, but in the microarray study conducted by Tasca et al. (2012).[44]

(G) As in C, but in the RNAseq study conducted by Wang et al. (2019).[15]

(H) As in C, but in the RNAseq study conducted by Yao et al. (2014).[41]

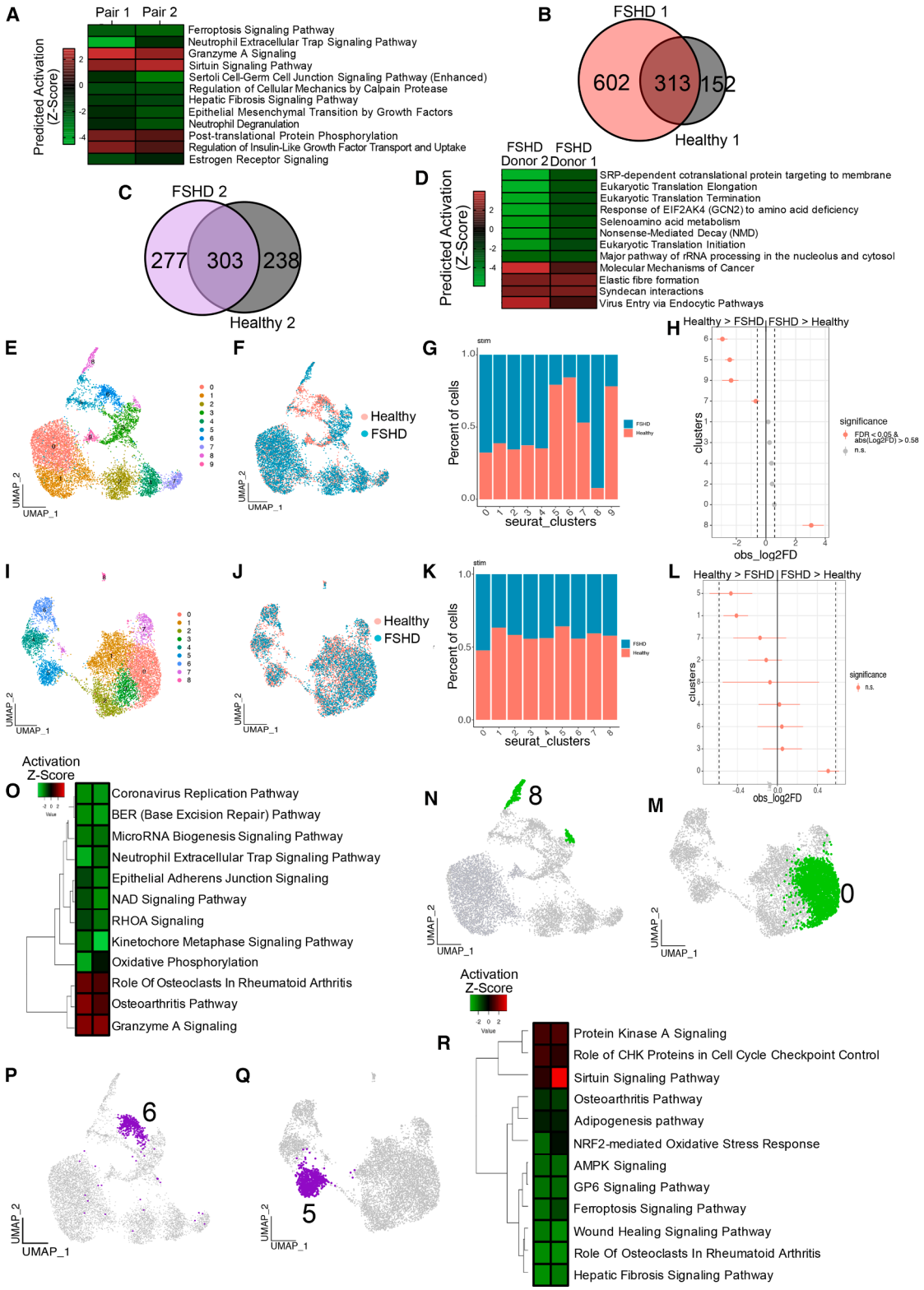

(legend on next page)

calpain protease, estrogen receptor, granzyme A, and Sirtuin signaling (all B-H corrected $p < 0.05$) (Figure 4A and Table S8). We also identified 602 genes in FSHD donor 1 and 277 genes in FSHD donor 2 that were DE only in FSHD myoblasts at 6-h relative to baseline (Figures 4B and 4C). Common dysregulated functional pathways across these FSHD-specific DE genes included SRP signaling, translation initiation, elongation, and termination pathways, nonsense-mediated decay, elastic fiber formation, syndecan interactions, and endocytosis pathways (Figure 4D and Table S9).

Using the scProportion Test on integrated FSHD and healthy samples, we found 1 cluster with a significantly greater proportion of FSHD than healthy myoblasts (cluster 8, FDR $p < 0.05$), and four clusters with proportionally fewer FSHD myoblasts (clusters 6, 5, 9, and 7, all FDR $p < 0.05$) in donor pair 1 at 6-h (Figures 4E–4H). In donor pair 2, cluster 0 tended to have a greater proportion of FSHD myoblasts, and cluster 5 tended to have fewer FSHD myoblasts, but no clusters reached significance (all FDR $p > 0.05$) (Figures 4I–4L). We performed a functional IPA analysis on the conserved markers from clusters with a greater proportion of FSHD myoblasts (cluster 8 in pair 1, and cluster 0 in pair 1, Figures 4M and 4N) and identified the top 12 pathways regulated in the same direction (*Z* score) in both clusters (Figure 4O). The pathways include DNA repair, neutrophil extracellular trap signaling, NAD signaling, oxidative phosphorylation, and granzyme A signaling (Table S10). In clusters containing the fewest FSHD myoblasts (cluster 6 in pair 1, and cluster 5 in pair 2, Figures 4P and 4Q) IPA analysis identified the enrichment of protein kinase A signaling, CHK protein cell cycle checkpoint, and sirtruin signaling, fibrosis, osteoclast activity, wound healing, and ferroptosis signaling (Figure 4R and Table S11).

FSHD myoblasts present with signs of ferroptotic stress before and after PM injury

As noted above, we observed significant enrichment of the Ferroptosis Signaling Pathway among differently expressed genes between FSHD and healthy myoblasts in both pairs (both FDR $p < 0.05$) (Figure 4A) at 6-h post-injury, including genes involved in the regulation of iron uptake, labile iron levels, polyunsaturated fatty acid deposition in membrane lipids, and the antioxidant system (Table S12). Furthermore, clusters with an over-representation of FSHD myoblasts at 6-h (clusters 8 in pair 1 and 0 in pair 2, Figures 4M–4O) demonstrated dysregulation of genes involved in the uptake of cysteine for glutathione biosynthesis (system Xc-) and lipid peroxidation[47–52] (Table S13). We also found the differential expression of key genes in the ferroptosis pathway between FSHD and healthy myoblasts at baseline (all FDR $p < 0.05$) (Table S12).

Based on these transcriptional findings, we investigated whether FSHD myoblasts display signs of ferroptotic stress, including accumulation of labile iron and increased lipid peroxidation. Using the fluorescent indicator of intracellular labile (Fe2+) iron FerroOrange, we found that labile iron was significantly elevated in FSHD ($n = 3$ donors) myoblasts compared to their healthy siblings ($n = 3$ donors) at baseline and 24-h post-injury ($p < 0.05$), but was significantly lower at 6-h post-injury ($p < 0.05$, Figures 5A and 5B). Since labile iron is highly reactive and promotes cell death through lipid peroxidation, we subsequently measured the level of lipid peroxidation using BODIPY 581/591 C11, which indicated FSHD cells have significantly greater levels of lipid peroxidation at baseline ($p < 0.05$), and 24-h post-injury ($p < 0.05$) (Figures 5C and 5D). We did not detect a difference in lipid peroxidation at 6-h post-injury (Figure 5D).

Figure 4. Unique transcriptional responses at 6-h post-injury in FSHD myoblasts

(A) The top 12 enriched functional pathways with predicted activation in the same direction from DE genes between FSHD and healthy myoblasts in each donor pair at 6-h post-injury (B-H corrected $p < 0.05$). Boxes are colored according to their predicted activation *Z* score (green tones = downregulated, red tones = upregulated, gray = no predicted *Z* score), scale to the left.

(B) Venn diagram showing the number of DE genes at 6-h relative to baseline in FSHD donor 1 myoblasts (red), and healthy donor 1 myoblasts (gray).

(C) DE genes for FSHD 2 myoblasts (purple), healthy donor 2 myoblasts (gray), and the number of DE genes in common.

(D) The top 12 significantly enriched functional pathways with predicted activation in the same direction from the unique DE genes from B and C (B-H corrected $p < 0.05$). Boxes are colored according to their predicted activation *Z* score (green = downregulated, red tones = upregulated, gray = no predicted *Z* score), scale to the left.

(E) Integrated UMAP of FSHD and healthy myoblasts from pair 1.

(F) UMAP of the distribution of FSHD (blue) and healthy (red) myoblasts in the UMAP from D.

(G) Histogram of the percentage of FSHD and healthy myoblasts in each cluster of the UMAP depicted in D.

(H) Results of the scProportionTest. X axis displays the log2fold-difference in abundance of healthy vs. FSHD myoblasts. Y axis lists the clusters in the UMAP. The dotted line denotes a log2FD in abundance of 0.58 (an increase or decrease in abundance of 1.5-fold). Clusters to the right of the 0 line have more FSHD than healthy myoblasts. Clusters to the left of the 0 line have more healthy than FSHD myoblasts. Whiskers denote the 95% confidence interval for the difference in proportions. Dots colored red denote clusters with significantly different proportions of FSHD vs. healthy myoblasts at FDR $p < 0.05$.

(I–L) Analysis as in A-D, but in donor pair 2.

(M) UMAP of donor pair 1 shows the location of cluster 8.

(N) UMAP of donor pair 2 shows the location of cluster 0.

(O) The top 12 significantly enriched functional pathways with predicted activation in the same direction in donor pair 1 cluster 8, and donor pair 2 cluster 0 from IPA (B-H corrected $p < 0.05$). Boxes are colored according to their predicted activation *Z* score (green tones = downregulated, red tones = upregulated, gray = no predicted *Z* score), scale in upper left.

(P) UMAP of donor pair 1 shows the location of cluster 6.

(Q) UMAP of donor pair 2 shows the location of cluster 5.

(R) The top 12 enriched functional pathways with predicted activation in the same direction in donor pair 1 cluster 6, and donor pair 2 cluster 5 from IPA (B-H corrected $p < 0.05$).

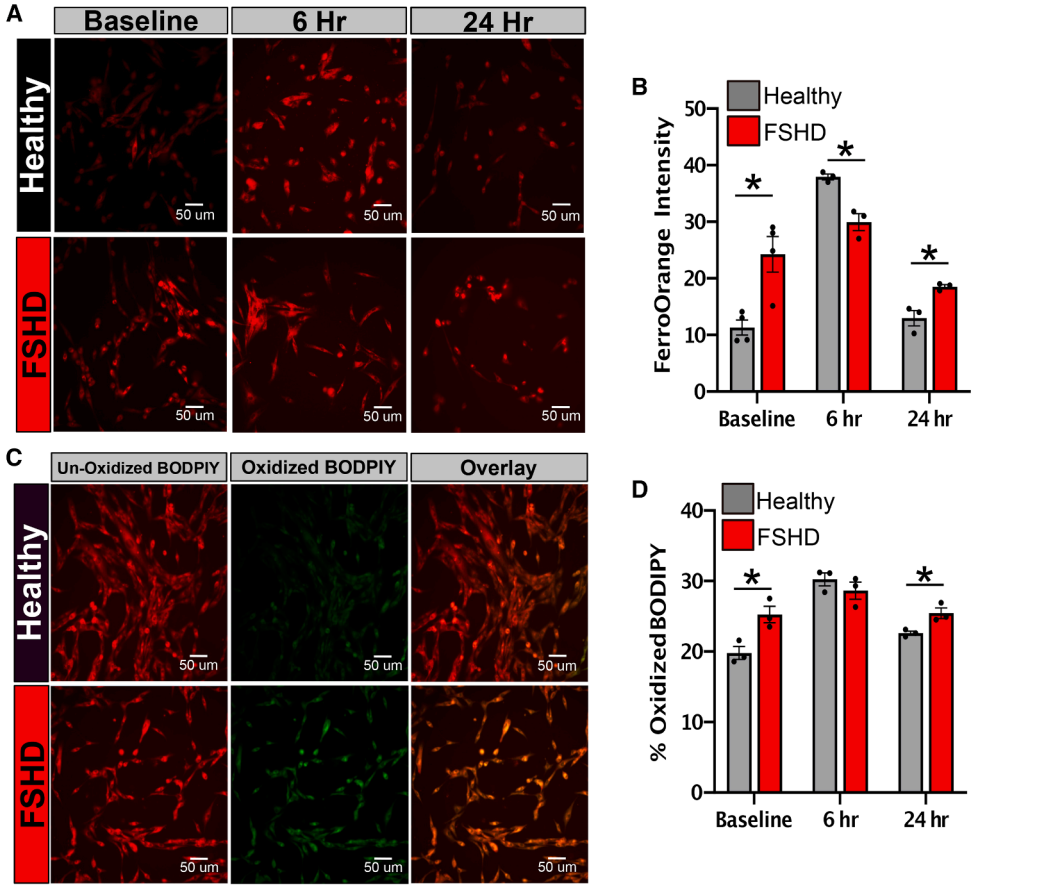

E

Study or Subgroup	FSHD Mean	FSHD SD	FSHD Total	Healthy Mean	Healthy SD	Healthy Total	Weight	Std. Mean Difference IV, Random, 95% CI
Dixit et al. (2007)	9.24	0.22	14	8.99	0.14	6	11.9%	1.19 [0.15, 2.23] *
Osborne et al. (2007)	7.12	0.1	19	7.03	0.13	30	21.9%	0.74 [0.15, 1.34] *
Rahimov et al. (2012)	7.59	0.075	26	7.56	0.087	24	23.0%	0.36 [-0.20, 0.92]
Tasca et al. (2012)	7.87	0.14	8	7.79	0.19	7	12.1%	0.46 [-0.58, 1.49]
Wang et al. (2019)	8.39	0.29	34	7.91	0.19	9	15.9%	1.72 [0.90, 2.55] ***
Yao et al. (2014)	9.36	0.23	15	9.31	0.06	8	15.2%	0.25 [-0.61, 1.11]
Total (95% CI)			**116**			**84**	**100.0%**	**0.76 [0.32, 1.19]**

Heterogeneity: Tau² = 0.13; Chi² = 9.36, df = 5 (P = 0.10); I² = 47%
Test for overall effect: Z = 3.39 (P = 0.0007)

Figure 5. Evidence of ferroptotic stress in FSHD myoblasts and human FSHD muscle biopsies

(A) Sample images of FerroOrange intensity in FSHD and healthy myoblasts at baseline (pre-injury), 6-, and 24-h post-injury.

(B) Quantification of FerroOrange intensity in FSHD myoblasts at baseline, 6-, and 24- hours post-injury (n = 3–4 FSHD and n = 3–4 healthy myoblast donor cell lines per timepoint). two-way ANOVA with genotype (FSHD vs. healthy) and time (baseline, 6-h, 24-h): significant interaction, $p = 0.006$. Post-hoc testing: * denotes $p < 0.05$ for the difference between FSHD and healthy myoblasts at each timepoint.

(C) Sample images of unoxidized BODIPY (red channel), oxidized BODIPY (green channel), and the overlayed image in healthy and FSHD myoblasts.

(D) Quantification of oxidized BOIPY at baseline, 6, and 24-h post-injury ($n = 3$ FSHD and $n = 3$ healthy donor cell lines per timepoint). Two ANOVA with genotype (FSHD vs. healthy) and time (baseline, 6-h, 24-h): significant interaction, $p = 0.007$. Post-hoc testing: * denotes $p < 0.05$ for the difference between FSHD and healthy myoblasts at each timepoint.

(E) Results of an inverse variance-weighted, random effects meta-analysis of the standardized mean difference in the ferroptosis severity score (FSS) in FSHD vs. healthy human muscle biopsies. For each study, the average and standard deviation (SD) of the FSS is listed for FSHD and healthy biopsies. The weight given to each study in the meta-analysis is listed, as well as the standard mean difference in FSS. The forest plot depicts the standard mean difference (location of green box), the weight (size of the green box), 95% confidence interval (CI) of the difference (whiskers) for each study, and the pooled standard mean difference (black diamond denoting pooled estimate and 95% CI). A standardized mean difference <0 indicates FSS is higher in healthy muscle biopsies. A standardized mean difference >0 indicates FSS is lower in healthy muscle biopsies. * denotes significant difference in FSS score in FSHD vs. healthy muscle biopsies (Mann-Whitney U test, *$p < 0.05$, **$p < 0.01$, and ***$p < 0.001$) in each individual study. All values are mean ± SEM.

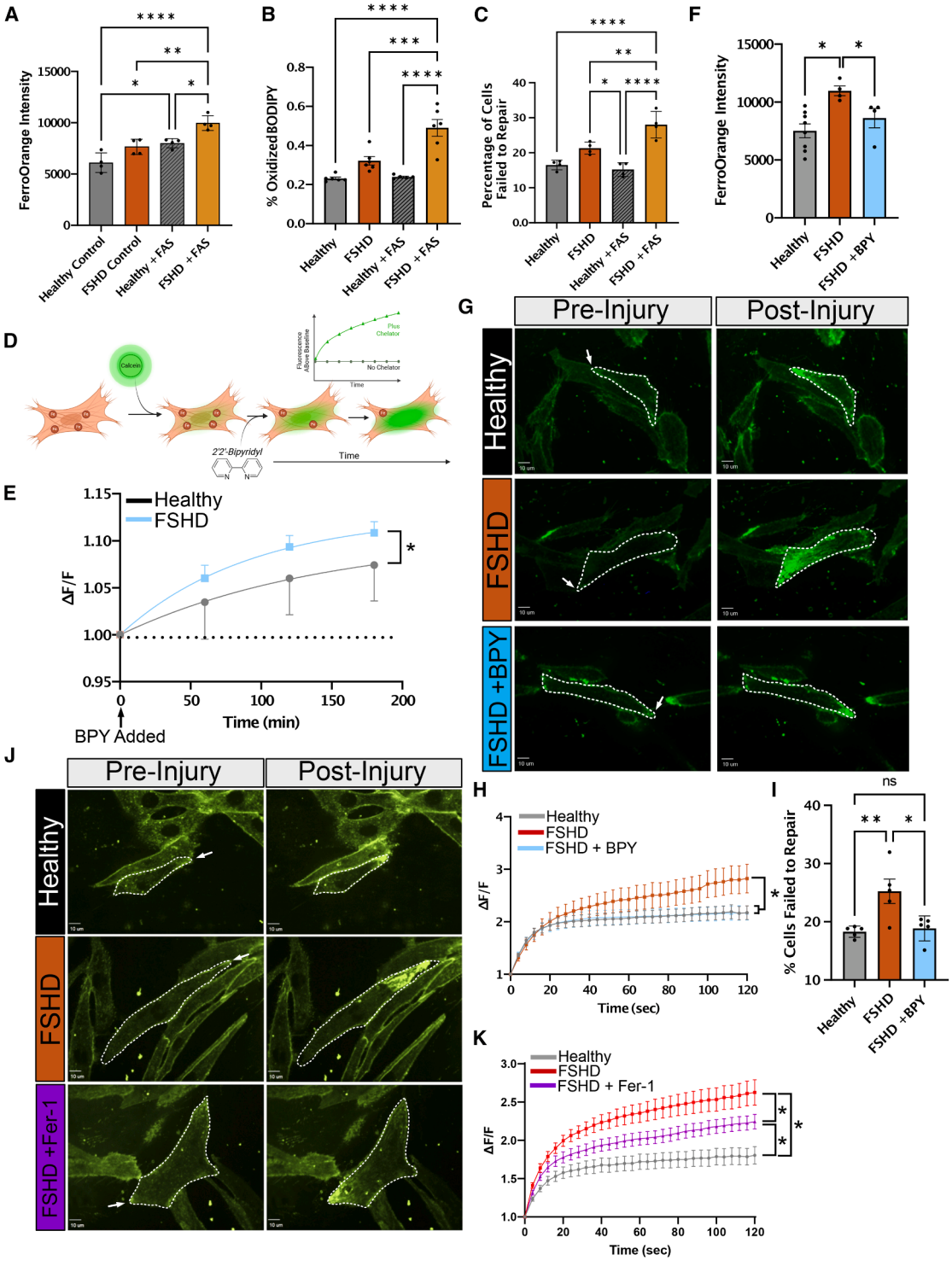

Figure 6. Role of labile iron in membrane repair deficits in FSHD

(A) Quantification of FerroOrange fluorescence intensity in untreated healthy and FSHD myoblasts, and myoblasts treated with 1 mM ferrous ammonium sulfate (FAS) for 24 h (n = 4 FSHD donors and n = 4 healthy donors). two-way ANOVA with genotype (FSHD, healthy), and treatment (untreated, FAS): main effects of genotype ($p < 0.001$) and treatment ($p < 0.001$). Post-hoc comparisons: * denotes $p < 0.05$, ** denotes $p < 0.01$, and *** denotes $p < 0.001$.

(B) Quantification of oxidized BODIPY as a measure of lipid peroxidation in untreated healthy and FSHD myoblasts, and myoblasts treated with 1 mM FAS for 24 h (n = 4 FSHD donors with 2 technical repeats for donors 1 and 2, n = 4 healthy donors with 2 technical repeats for donors 1 and 2). two-way ANOVA with genotype

(legend continued on next page)

Expression of ferroptosis biomarkers is elevated in FSHD muscle biopsies and is predictive of skeletal muscle inflammation

To determine if human FSHD muscle biopsies display transcriptional signs of ferroptotic stress, we calculated a ferroptotic stress score (FSS) based on the average expression of previously validated markers of ferroptosis (*PTGS2, NFE2L2, SLC40A1, SLC7A11, AKR1C1, FTH1, TXNRD1, CHAC1, ABCC1, MT1G, NQO1, CBS, HMOX1*)[53] in FSHD muscle biopsies collected by Yao et al. (2014)[41]; Rahimov et al. (2012)[42]; Dixit et al. (2007)[3]; Wang et al. (2019)[15]; Osborne et al. (2007)[43]; and Tasca et al. (2012).[44] The FSS scores were significantly elevated in 3 of 6 individual studies, but elevated in FSHD samples in all studies (Figure 5E). We summarized these scores across 116 FSHD and 84 healthy biopsies using an inverse variance, random effects meta-analysis, which indicated FSHD biopsies have significantly elevated expression of ferroptotic stress biomarkers (pooled standard mean difference in FSS of 0.76 (0.32, 1.20), z = 3.39, $p < 0.001$) (Figure 5E). The FSS score was also elevated in donor pair 2 FSHD myoblasts at baseline, and at 6-h post injury (both $p < 0.001$), but not in donor pair 1 FSHD myoblasts ($p > 0.05$).

Since previous studies have linked ferroptotic stress and ferroptotic cell death to the release of damage-associated molecular patterns (DAMPs) and tissue inflammation,[54] we subsequently evaluated if the expression of these genes was related to histological evidence of inflammatory infiltration in the muscle samples collected by Wang et al. (2019).[15] Binary logistic regression indicated that the Ferroptosis Stress Score was a significant predictor of skeletal muscle inflammation in FSHD muscle biopsies after controlling for age, sex, and repeat length ($p = 0.009$), with a one unit increase in the Ferroptosis Stress Score associated with 7.625 times greater log odds of having skeletal muscle inflammation (b = 7.624 (2.92), Table S14). Furthermore, we found significant positive spearman rho coefficients between ferroptosis score and T1 score (rating the amount of fat deposition on a scale from 0 to 5 from normal appearance to pervasive fatty replacement throughout the muscle using MRI) (rho = 0.365, $p = 0.034$), as well as the STIR score (a separate measure of muscle inflammation obtained from MRI, rho = 0.364, $p = 0.034$).[15]

CHELATION OF LABILE IRON AND TREATMENT WITH FERROPTOSIS INHIBITOR FERROSTATIN-1 IMPROVES PM REPAIR CAPACITY IN FSHD MYOBLASTS

To determine if elevated levels of labile iron contribute to membrane repair deficits in FSHD, we induced ferroptotic stress by increasing the labile iron pool via treatment with 1 mM ferrous ammonium sulfate (FAS) for 24 h. FAS treatment increased labile iron levels in healthy and FSHD myoblasts, but the increase was significantly greater in FSHD, suggesting underlying deficits in labile iron metabolism ($p < 0.05$, Figure 6A). Unlike labile iron, FAS treatment increased lipid peroxidation only in FSHD myoblasts (Figure 6B, $p < 0.05$). Scrape-injuring FSHD myoblasts following FAS treatment results in a greater percentage of PI(+) cells, which was not observed in healthy myoblasts ($p < 0.05$, Figure 6C). Taken together, these results suggest FSHD myoblasts have a reduced capacity to respond to perturbations in labile iron.

To confirm that elevated levels of labile iron and lipid peroxidation are detrimental to membrane repair in FSHD, we treated FSHD myoblasts with the iron chelator 2,2′-bipyridyl (BPY). To determine the time-course of iron chelation following treatment with BPY, we loaded FSHD and healthy myoblasts with 2 μM cell-permeant fluorescent calcein AM green, which is quenched by labile iron (Figure 6D). Following treatment with BPY, labile iron chelation de-quenches calcein, leading to an increase in GFP fluorescence (Figure 6D). We confirmed that treatment with 1 mM BPY for as little as 3 h significantly reduced labile

(FSHD, healthy), and treatment (untreated, FAS): significant interaction ($p = 0.005$). Post-hoc comparisons: * denotes $p < 0.05$, ** denotes $p < 0.01$, and *** denotes $p < 0.001$.

(C) Percentage of cells that failed to repair using the acute cell death assay (Figure 1) in untreated healthy and FSHD myoblasts, and myoblasts treated with 1 mM FAS for 24 h ($n = 4$ FSHD and $n = 4$ healthy donor cell lines). two-way ANOVA with genotype (FSHD, healthy), and treatment (untreated, FAS): significant interaction ($p = 0.003$). Post-hoc comparisons: * denotes $p < 0.05$, ** denotes $p < 0.01$, and *** denotes $p < 0.001$.

(D) Diagram of the iron chelation assay confirms the time-course of 2,2′-Bipyridyl (BPY) chelation in human myoblasts. Briefly, myoblasts were loaded with 2 μM cell-permeant, calcein AM green, which is quenched by cytosolic labile iron. Treatment with BPY chelates labile iron, de-quenches calcein, and increases green fluorescence signal over time.

(E) Kinetics of calcein fluorescence in healthy (gray) and FSHD (light red) myoblasts following treatment with 1 mM BPY for 180 min. two-way ANOVA with genotype (FSHD, healthy), and time (0, 60, 120, 180 min): significant main effect of genotype ($p = 0.01$). * denotes $p < 0.05$.

(F) Quantification of FerroOrange fluorescence intensity in untreated healthy and FSHD myoblasts, and myoblasts treated with 1 mM BPY for 3 h ($n = 4$ healthy donors with 1 technical replicate for each line, $n = 4$ FSHD donor cell lines). One-Way ANOVA: $p = 0.01$. Multiple comparisons: * denotes $p < 0.05$.

(G) Images of FM1-43 dye entry (green) in injured, untreated myoblasts at baseline (pre-injury) and at 120 s post-injury, as well as myoblasts treated with 1 mM BPY for 3 h. The arrow indicates the location of the laser injury. The dotted line indicates the cell outline.

(H) Kinetics of intracellular FM1-43 dye fluorescence intensity (ΔF/F) over time for healthy (donor 1, $n = 18$), FSHD (donor 1, $n = 19$), and BPY-treated FSHD (donor 1, $n = 17$) myoblasts. Greater dye entry indicates worse repair. Two-Way ANOVA with genotype (FSHD vs. healthy) and time (0–120 s): significant main effects of group ($p < 0.001$) and time ($p < 0.001$). Post-hoc testing: * denotes FSHD + BPY and healthy significantly less than untreated FSHD from 100 to 120 s $p < 0.05$.

(I) Quantification of the percentage of cells that failed to repair acute scrape injury in untreated healthy and FSHD myoblasts, and BPY-treated FSHD myoblasts. One-Way ANOVA: $p < 0.006$. Multiple comparisons: * denotes $p < 0.05$, ** denotes $p < 0.01$, and *** denotes $p < 0.001$.

(J) Images of FM1-43 dye entry (green) in injured, untreated myoblasts at baseline (pre-injury) and at 120 s post-injury, as well as myoblasts treated with 100 μM Ferrostatin for 24-h. The arrow indicates the location of the laser injury. Dotted line indicates the cell outline.

(K) Kinetics of intracellular FM1-43 dye fluorescence intensity (ΔF/F) over time for healthy (donors 1 and 2, $n = 29$), FSHD (donors 1 and 2, $n = 29$), and ferrostatin-treated FSHD (donor 1&2, $n = 31$) myoblasts. Greater dye entry indicates worse repair. two-Way ANOVA with genotype (FSHD vs. healthy) and time (0–120 s): significant interaction ($p < 0.001$). * denotes all groups different from 86 to 120 s, $p < 0.05$. All values are mean ± SEM.

iron levels, and that the increase in calcein fluorescence intensity was greater in FSHD vs. healthy myoblasts (Figure 6E, $p < 0.05$), reflective of their elevated labile iron pool. These findings were confirmed using FerroOrange in FSHD cells, with BPY reducing FO fluorescence intensity toward healthy myoblast levels ($p < 0.05$, Figure 6F). Furthermore, treatment with 1 mM BPY for 3 h resulted in significant improvements in PM repair in FSHD myoblasts, as well as a reduction in the percentage of cells that fail to repair acute scrape injury (Figure 6G, 6H, and 6I, $p < 0.05$). Finally, we treated FSHD myoblasts with ferroptosis inhibitor ferrostatin-1—a radical-trapping antioxidant that reduces lipid peroxides. Treatment with 100 μM ferrostatin-1 for 24 h significantly improved membrane repair in FSHD myoblasts (Figure 6J, and 6K, $p < 0.05$). Taken together, these data show that FSHD myoblasts have poor tolerance for elevated labile iron levels and that lipid peroxidation secondary to elevated labile iron may contribute to PM repair deficits previously identified in FSHD.

DISCUSSION

In this study, we provide evidence of increased DUX4 and DUX4-target gene expression 6-h after PM injury in FSHD myoblasts, which remains elevated through 24-h.[45,55] However, the level of DUX4 expression and its downstream targets was significantly lower than those observed following myoblast differentiation—a frequently used approach to stimulate detectable increases in endogenous DUX4.[26,56–58] Therefore, the effects of DUX4 expression triggered by PM injury, as identified in this study, may provide unique insight into the effects of DUX4 expression below those previously reported.

To this end, we generated lists of genes consistently upregulated in both FSHD myoblast donors compared to their healthy siblings at baseline and 6-h post-injury. Despite small fold changes in several genes, meta-analysis of human FSHD muscle biopsies indicated these gene signatures were more highly expressed in FSHD muscles, and were highly sensitive and specific classifiers of FSHD. IPA analysis of our baseline signature indicated FSHD myocytes may be in a state of heightened stress, denoted by predicted activation of pathways involved in translational regulation and ribosomal RNA processing, active protein processing (e.g., nonsense-mediated decay), restoration of membrane components and secretory functions, cell cycle pausing, diminished mtRNA surveillance, and reduced immune interactions. Importantly, genes in our 6-h signature were the most differently expressed between FSHD and healthy human muscle biopsies (based on p-value)—suggesting FSHD muscles show transcriptional similarities to cells recovering from membrane injury. These genes were enriched in pathways critical for membrane repair (such as ATP generation/OXPHOS[59]), and satellite cell proliferation and differentiation during regeneration (including degradation of the extracellular matrix, integrin interactions, and syndecan interactions[60–62]).

Our 6-h pseudobulk analysis further identified transcriptional signs of elevated stress in FSHD vs. healthy myoblasts post-injury that are consistent with the suppression of translational activity, reduction of non-essential cell functions (reduced membrane protein targeting and ribosome biogenesis), impaired stress responses (downregulation of GCN2 pathway), reduced antioxidant capacity (downregulation of selenoaminoacid metabolism), and increased vulnerability to proteotoxic stress (downregulation of nonsense-mediated decay). Indeed, our proportion analysis indicated that FSHD myoblasts were over-represented in clusters presenting with transcriptional signs of dysfunctional homeostasis, including reduced genomic integrity (e.g., reduced base excision repair activity), mitigated communication with the immune system (e.g., reduced neutrophil extracellular trap signaling), reduced energy metabolism (e.g., nicotinamide adenine dinucleotide signaling, OXPHOS), and reduced cytoskeletal cell motility (e.g., adherens junction signaling). The positive correlations between the expression of our baseline and 6-h gene signatures with histopathologic evidence of fiber size variability, centrally located nuclei, interstitial fibrosis, and muscle fiber necrosis/regeneration/inflammation, expression of DUX4 downstream targets, and their elevated expression at 6-h post-injury when DUX4 expression is highest, further suggest these genes are responsive to increases in disease severity.

Importantly, one of the top enriched pathways in DE genes in our pseudobulk analysis at 6-h post-injury was the Ferroptosis pathway. Ferroptosis is a recently discovered non-apoptotic form of programmed cell death driven by the accumulation of lipid peroxidation, which increases membrane curvature and induces oxidative micellization and pore formation, leading to cell death.[63] The loss of iron homeostasis and ferroptosis have been implicated in the onset of multiple neuromuscular diseases, including amytrophic lateral sclerosis (ALS),[64] sarcopenia,[65] Duchenne muscular dystrophy,[66] and rhabdomyolysis.[67] Our proportion analysis also identified dysregulation of the ferroptosis pathway in clusters with an over-representation of FSHD myoblasts, including the downregulation of genes in system Xc-, upregulation of genes that augment lipid peroxidation, and downregulation of genes that limit lipid peroxidation—transcriptional changes that would be expected to increase ferroptotic stress.[63] Transcriptional changes in genes regulating lipid peroxidation, iron uptake and storage, antioxidant defenses, and formation of polyunsaturated fatty acids were also detected in uninjured FSHD myoblasts compared to their healthy siblings.

Since the identification of ferroptosis requires a combination of transcription/protein, morphological, and biochemical measures, we further examined myoblasts for levels of labile iron and lipid peroxidation. We found FSHD myoblasts present with elevated labile iron and lipid peroxidation pre-injury and 24-h post-injury. These findings coincide with evidence of iron accumulation in human FSHD muscle biopsies and in muscle from a skeletal-muscle-specific transgenic mouse model of FSHD reported by Nakamura et al. (2025).[36]

At 6-h post-injury, we observed a significant increase in labile iron and lipid peroxidation in both FSHD and healthy myoblasts, which returns to baseline by 24-h—indicating this may be a physiological response to increase intracellular iron after injury. Previous studies have reported that iron uptake is required for satellite cell activation, proliferation, and fusion during muscle regeneration.[68–70] Moreover, skeletal muscle increases the expression of ferritin receptors and transferrin post-injury,[71] which is indispensable for muscle regeneration,[69] and is facilitated via iron recycling and secretion by infiltrating

macrophages.[68] The lower labile iron levels we observed at 6-h post-injury in FSHD myoblasts may be indicative of deficits in iron uptake during recovery. This could potentially compromise their activation, proliferation, or differentiation during regeneration—but this requires further investigation.

We found that augmenting labile iron levels in FSHD myoblasts worsens cell survival in response to PM injury, while iron chelation improves survival, suggesting that iron overload may be a contributor to poor membrane repair and/or cell death in FSHD. Ikeda et al. (2019) previously reported that elevated labile iron increases cell death and suppresses myogenesis *in vivo* secondary to elevated oxidative stress.[72] Likewise, we observed significant improvement in membrane repair kinetics in response to Fer-1, a radical-trapping antioxidant that reduces lipid peroxides, which further suggests ferroptotic stress mitigates membrane repair.

Importantly, these results conflict with the *in vitro* and *in vivo* results from Nakamura et al. (2025),[36] who reported that treatment with FAS for 48 h did not change iron granule content but was protective from the effects of DUX4 based on evidence of improved FSHD myotube morphology. In contrast, iron chelation reduced labile iron but did not improve myotube morphology. These differences could be due to multiple reasons, including the use of myotubes (Nakamura et al. 2025)[36] vs. myoblasts (our study), different treatment concentrations and durations of FAS, use of different iron chelators (DFO vs. BPY), and the use of primary mouse myoblasts (Nakamura et al. 2025)[36] vs. primary immortalized human myoblasts (our study). However, the authors did report similar results following treatment with ferrostatin-1, showing it was effective against DUX4 cytotoxicity—coinciding with our evidence of elevated ferroptotic stress in FSHD cells and tissues. Indeed, the results of our study provide important insight into the behavior of satellite cells or myoblasts following injury in the context of endogenous DUX4 expression.

Previous studies have found evidence for elevated lipid peroxidation and oxidative damage in FSHD muscle biopsies,[14] as well as DUX4-induced mitochondrial dysfunction via inhibition of complex I,[32] and iron accumulation (Nakamura et al., 2025).[36] Inhibition of complex I was also previously shown to sensitize cells to ferroptosis.[73] In contrast to the results of Nakamura et al. (2025),[36] our lab recently published evidence of elevated mitochondrial iron in FSHD myoblasts, which may further exacerbate oxidative stress and provide an additional source of iron for Fenton reactions.[33] Moreover, cells undergoing ferroptosis often develop smaller mitochondria without cristae and a condensed membrane—morphological features also identified in FSHD skeletal muscles.[74] Our meta-analysis demonstrated that the expression of marker genes for ferroptosis/ferroptotic-stress is elevated in FSHD compared to healthy muscle, and that their expression was: 1) a positive predictor of histological evidence of muscle inflammation and 2) positively associated with radiological signs of fatty infiltration and inflammation in FSHD muscles. However, further biochemical evaluation of FSHD muscle biopsies is warranted to confirm the role of ferroptosis in human FSHD muscle.

Inflammation is one of the earliest characterized features of affected muscle, and often precedes histological or radiographic signs of disease.[24,75] The precipitating events leading to muscle inflammation are poorly defined in FSHD, but previous studies have implicated DUX4-induced inhibition of nonsense-mediated decay, which triggers the release of DAMPs, as well as increased expression of complement component RNAs.[44,76] Ferroptosis is associated with the release of DAMPs such as high-mobility group box 1 (HMGB1), and lipid oxidation products that can stimulate inflammatory immune responses.[77] Ferroptosis or ferroptotic stress in response to DUX4 expression, membrane injury, or both, may therefore also be a contributing factor to the onset and progression of inflammatory and fibrotic lesions in FSHD. Several iron chelators have already been approved for the treatment of beta-thalassemia and other iron overload conditions, including deferoxamine (Desferal), deferasirox (Exjade), and deferiprone (Ferirprox).[78] Treatment with deferiprone in the *mdx* mouse model of DMD, which also presents with elevated iron in the severely dystrophic diaphragm muscle, was previously reported to reduce iron levels, oxidative stress, and fibrosis.[79] However, it should be noted that the recent study by Nakamura et al. (2025) found iron supplementation via high iron diet or the drug ferric carboxymaltose (FCM) unexpectedly reduced iron accumulation while improving treadmill running performance, increasing grip strength, preventing muscle damage, and reducing the expression of genes in the ferroptosis pathway in a mouse model of FSHD.[36] Despite the differences between our study and ([36]), both studies found phenotypic and molecular improvements with ferroptosis inhibition – further confirming a need to define the mechanisms of ferroptosis in FSHD, and to consider this pathway as a target for therapy.

Limitations of the study

In this study we used scRNAseq, which is associated with several limitations, including biases in transcript coverage, sequencing coverage, and low capture efficiency. scRNA-seq data typically have a higher degree of noise compared to bulk RNA-seq data.[80] However, we used robust data quality control, normalization, and differential expression approaches to identify transcriptional changes between cells and conditions and limit bias. We also limited our analyses to differences appearing between FSHD and healthy siblings in both donor pairs to focus on consistent differences associated with FSHD.

Additionally, we have limited our analysis of ferroptosis to FSHD primary immortalized myoblasts, which may display differences in iron metabolism and ferroptosis activation from myotubes or myofibers. Although we found transcriptional evidence of increased expression of Ferroptosis biomarkers in FSHD muscle biopsies, further biochemical analysis of ferroptotic stress, including elevated labile iron and lipid peroxidation, is warranted in FSHD tissues to confirm our findings.

Finally, while our baseline and 6-h post-injury gene signatures were significantly elevated across 166 FSHD vs. 84 healthy muscle biopsies, they were not significantly different in all external muscle biopsy datasets. There are many potential reasons for a gene set to not validate in every external sample, including natural biological variability, technical measurement errors (sample handling, storage, assay issues such as different isoforms), statistical challenges (overfitting in small datasets), flaws in study design (selection bias, confounding factors such as diet/age),

or other fundamental complexities (the marker reflecting different stages or being affected by treatment, not just disease). Since multiple biomarkers are typically combined when making clinical decisions, we would recommend the same approach in the development of biomarkers for FSHD.

RESOURCE AVAILABILITY

Lead contact

Requests for further information and resources should be directed to and will be fulfilled by the lead contact, Yi-Wen Chen, ychen@childrensnational.org.

Materials availability

This study did not generate new unique reagents.

Data and code availability

The scRNAseq data generated during this study have been deposited in the NCBI Gene Expression Omnibus (accession number GSE303359) and are publicly available as of the date of publication. This paper does not report original code. Any additional information required to reanalyze the data reported in this paper is available from the lead contact upon request.

ACKNOWLEDGMENTS

We would like to thank Dr. Karuna Panchapakesan and Dr. Susan Knoblach (Center for Genetic Medicine, Genomics and Bioinformatics Core, Children's National Hospital, Washington, DC, USA) for their assistance with the processing of single-cell RNA sequencing samples. This research was supported by the National Institutes of Health T32 AR056993-06 (Partridge) and 1R21HD103993-01 (Chen), as well as the Muscular Dystrophy Association—Strength, Science, and Stories of Inspiration Fellowship (A. Bittel), FSHD Canada (Chen), an FSHD Society Grant Award (A. Bittel), the American Physical Therapy Association New Investigator Fellowship Training Initiative (A. Bittel), and an MDA Development Grant (A. Bittel).

AUTHOR CONTRIBUTIONS

A.J.B. and Y.W.C. conceived and designed the study; A.J.B., S.B., and L.O. conducted data analysis; A.J.B., Y.W.C., S.B., and L.O. performed data interpretation; A.J.B. drafted the manuscript, which was edited by all authors; A.J.B. and Y.W.C. obtained funding for the study.

DECLARATION OF INTERESTS

The authors declare no competing interests.

STAR★METHODS

Detailed methods are provided in the online version of this paper and include the following:

- KEY RESOURCES TABLE
- EXPERIMENTAL MODEL AND STUDY PARTICIPANT DETAILS
  - Cell culture
- METHOD DETAILS
  - Cell injury assays
  - Cell treatments
  - Acute cell death assay
  - Iron chelation assay
  - Single cell transcriptomics platform: 10x chromium
  - scRNA-sequencing and processing of 10x genomics chromium scRNA-seq data
  - Functional annotations
  - Live cell imaging
  - RNA isolation, RT-PCR, digital PCR
  - Published gene expression data and calculation of ferroptosis severity score
- QUANTIFICATION AND STATISTICAL ANALYSIS

SUPPLEMENTAL INFORMATION

Supplemental information can be found online at https://doi.org/10.1016/j.isci.2026.115781.

Received: October 7, 2025
Revised: April 12, 2026
Accepted: April 15, 2026
Published: April 17, 2026

REFERENCES

1. Lunt, P.W., Compston, D.A., and Harper, P.S. (1989). Estimation of age dependent penetrance in facioscapulohumeral muscular dystrophy by minimising ascertainment bias. J. Med. Genet. *26*, 755–760. https://doi.org/10.1136/jmg.26.12.755.
2. Mah, J.K., and Chen, Y.W. (2018). A Pediatric Review of Facioscapulohumeral Muscular Dystrophy. J. Pediatr. Neurol. *16*, 222–231. https://doi.org/10.1055/s-0037-1604197.
3. Dixit, M., Ansseau, E., Tassin, A., Winokur, S., Shi, R., Qian, H., Sauvage, S., Mattéotti, C., van Acker, A.M., Leo, O., et al. (2007). *DUX4* , a candidate gene of facioscapulohumeral muscular dystrophy, encodes a transcriptional activator of *PITX1*. Proc. Natl. Acad. Sci. USA *104*, 18157–18162. https://doi.org/10.1073/pnas.0708659104.
4. Lemmers, R.J.L.F., de Kievit, P., Sandkuijl, L., Padberg, G.W., van Ommen, G.J.B., Frants, R.R., and van der Maarel, S.M. (2002). Facioscapulohumeral muscular dystrophy is uniquely associated with one of the two variants of the 4q subtelomere. Nat. Genet. *32*, 235–236. https://doi.org/10.1038/ng999.
5. Lemmers, R.J.L.F., van der Vliet, P.J., Klooster, R., Sacconi, S., Camaño, P., Dauwerse, J.G., Snider, L., Straasheijm, K.R., van Ommen, G.J., Padberg, G.W., et al. (2010). A Unifying Genetic Model for Facioscapulohumeral Muscular Dystrophy. Science *329*, 1650–1653. https://doi.org/10.1126/science.1189044.
6. Wijmenga, C., Hewitt, J.E., Sandkuijl, L.A., Clark, L.N., Wright, T.J., Dauwerse, H.G., Gruter, A.M., Hofker, M.H., Moerer, P., and Williamson, R. (1992). Chromosome 4q DNA rearrangements associated with facioscapulohumeral muscular dystrophy. Nat. Genet. *2*, 26–30. https://doi.org/10.1038/ng0992-26.
7. Hamanaka, K., Šikrová, D., Mitsuhashi, S., Masuda, H., Sekiguchi, Y., Sugiyama, A., Shibuya, K., Lemmers, R.J.L.F., Goossens, R., Ogawa, M., et al. (2020). Homozygous nonsense variant in *LRIF1* associated with facioscapulohumeral muscular dystrophy. Neurology *94*, e2441–e2447. https://doi.org/10.1212/WNL.0000000000009617.
8. Lemmers, R.J.L.F., Tawil, R., Petek, L.M., Balog, J., Block, G.J., Santen, G.W.E., Amell, A.M., van der Vliet, P.J., Almomani, R., Straasheijm, K.R., et al. (2012). Digenic inheritance of an SMCHD1 mutation and an FSHD-permissive D4Z4 allele causes facioscapulohumeral muscular dystrophy type 2. Nat. Genet. *44*, 1370–1374. https://doi.org/10.1038/ng.2454.
9. Strafella, C., Caputo, V., Bortolani, S., Torchia, E., Megalizzi, D., Trastulli, G., Monforte, M., Colantoni, L., Caltagirone, C., Ricci, E., et al. (2023). Whole exome sequencing highlights rare variants in CTCF, DNMT1, DNMT3A, EZH2 and SUV39H1 as associated with FSHD. Front. Genet. *14*, 1235589. https://doi.org/10.3389/fgene.2023.1235589.
10. Knopp, P., Krom, Y.D., Banerji, C.R.S., Panamarova, M., Moyle, L.A., den Hamer, B., van der Maarel, S.M., and Zammit, P.S. (2016). DUX4 induces a transcriptome more characteristic of a less-differentiated cell state and inhibits myogenesis. J. Cell Sci. *129*, 3816–3831. https://doi.org/10.1242/jcs.180372.

11. Resnick, R., Wong, C.J., Hamm, D.C., Bennett, S.R., Skene, P.J., Hake, S.B., Henikoff, S., van der Maarel, S.M., and Tapscott, S.J. (2019). DUX4-Induced Histone Variants H3.X and H3.Y Mark DUX4 Target Genes for Expression. Cell Rep. *29*, 1812–1820.e5. https://doi.org/10.1016/j.celrep.2019.10.025.

12. Van Der Maarel, S.M., Tawil, R., and Tapscott, S.J. (2011). Facioscapulohumeral muscular dystrophy and DUX4: breaking the silence. Trends Mol. Med. *17*, 252–258. https://doi.org/10.1016/j.molmed.2011.01.001.

13. Bosnakovski, D., Toso, E.A., Hartweck, L.M., Magli, A., Lee, H.A., Thompson, E.R., Dandapat, A., Perlingeiro, R.C.R., and Kyba, M. (2017). The DUX4 homeodomains mediate inhibition of myogenesis and are functionally exchangeable with the Pax7 homeodomain. J. Cell Sci. *130*, 3685–3697. https://doi.org/10.1242/jcs.205427.

14. Turki, A., Hayot, M., Carnac, G., Pillard, F., Passerieux, E., Bommart, S., Raynaud de Mauverger, E., Hugon, G., Pincemail, J., Pietri, S., et al. (2012). Functional muscle impairment in facioscapulohumeral muscular dystrophy is correlated with oxidative stress and mitochondrial dysfunction. Free Radic. Biol. Med. *53*, 1068–1079. https://doi.org/10.1016/j.freeradbiomed.2012.06.041.

15. Wang, L.H., Friedman, S.D., Shaw, D., Snider, L., Wong, C.J., Budech, C.B., Poliachik, S.L., Gove, N.E., Lewis, L.M., Campbell, A.E., et al. (2019). MRI-informed muscle biopsies correlate MRI with pathology and DUX4 target gene expression in FSHD. Hum. Mol. Genet. *28*, 476–486. https://doi.org/10.1093/hmg/ddy364.

16. Ciszewski, L., Lu-Nguyen, N., Slater, A., Brennan, A., Williams, H.E.L., Dickson, G., Searle, M.S., and Popplewell, L. (2020). G-quadruplex ligands mediate downregulation of DUX4 expression. Nucleic Acids Res. *48*, 4179–4194. https://doi.org/10.1093/nar/gkaa146.

17. Haynes, P., Kernan, K., Zhou, S.L., and Miller, D.G. (2017). Expression patterns of FSHD-causing DUX4 and myogenic transcription factors PAX3 and PAX7 are spatially distinct in differentiating human stem cell cultures. Skelet. Muscle *7*, 13. https://doi.org/10.1186/s13395-017-0130-1.

18. Sasaki-Honda, M., Jonouchi, T., Arai, M., Hotta, A., Mitsuhashi, S., Nishino, I., Matsuda, R., and Sakurai, H. (2018). A patient-derived iPSC model revealed oxidative stress increases facioscapulohumeral muscular dystrophy-causative DUX4. Hum. Mol. Genet. *27*, 4024–4035. https://doi.org/10.1093/hmg/ddy293.

19. Banerji, C.R.S., Panamarova, M., Hebaishi, H., White, R.B., Relaix, F., Severini, S., and Zammit, P.S. (2017). PAX7 target genes are globally repressed in facioscapulohumeral muscular dystrophy skeletal muscle. Nat. Commun. *8*, 2152. https://doi.org/10.1038/s41467-017-01200-4.

20. McNeil, P.L., and Khakee, R. (1992). Disruptions of muscle fiber plasma membranes. Role in exercise-induced damage. Am. J. Pathol. *140*, 1097–1109.

21. Dias, C., and Nylandsted, J. (2021). Plasma membrane integrity in health and disease: significance and therapeutic potential. Cell Discov. *7*, 4. https://doi.org/10.1038/s41421-020-00233-2.

22. Bittel, A.J., Sreetama, S.C., Bittel, D.C., Horn, A., Novak, J.S., Yokota, T., Zhang, A., Maruyama, R., Rowel Q Lim, K., Jaiswal, J.K., and Chen, Y.W. (2020). Membrane Repair Deficit in Facioscapulohumeral Muscular Dystrophy. IJMS *21*, 5575. https://doi.org/10.3390/ijms21155575.

23. Horn, A., and Jaiswal, J.K. (2018). Cellular mechanisms and signals that coordinate plasma membrane repair. Cell. Mol. Life Sci. *75*, 3751–3770. https://doi.org/10.1007/s00018-018-2888-7.

24. Banerji, C.R.S., Henderson, D., Tawil, R.N., and Zammit, P.S. (2020). Skeletal muscle regeneration in facioscapulohumeral muscular dystrophy is correlated with pathological severity. Hum. Mol. Genet. *29*, 2746–2760. https://doi.org/10.1093/hmg/ddaa164.

25. Dandapat, A., Bosnakovski, D., Hartweck, L.M., Arpke, R.W., Baltgalvis, K.A., Vang, D., Baik, J., Darabi, R., Perlingeiro, R.C.R., Hamra, F.K., et al. (2014). Dominant lethal pathologies in male mice engineered to contain an X-linked DUX4 transgene. Cell Rep. *8*, 1484–1496. https://doi.org/10.1016/j.celrep.2014.07.056.

26. Rickard, A.M., Petek, L.M., and Miller, D.G. (2015). Endogenous DUX4 expression in FSHD myotubes is sufficient to cause cell death and disrupts RNA splicing and cell migration pathways. Hum. Mol. Genet. *24*, 5901–5914. https://doi.org/10.1093/hmg/ddv315.

27. Wallace, L.M., Garwick, S.E., Mei, W., Belayew, A., Coppee, F., Ladner, K.J., Guttridge, D., Yang, J., and Harper, S.Q. (2011). DUX4, a candidate gene for facioscapulohumeral muscular dystrophy, causes p53-dependent myopathy in vivo. Ann. Neurol. *69*, 540–552. https://doi.org/10.1002/ana.22275.

28. Bosnakovski, D., Gearhart, M.D., Toso, E.A., Ener, E.T., Choi, S.H., and Kyba, M. (2018). Low level DUX4 expression disrupts myogenesis through deregulation of myogenic gene expression. Sci. Rep. *8*, 16957. https://doi.org/10.1038/s41598-018-35150-8.

29. Mariot, V., Joubert, R., Le Gall, L., Sidlauskaite, E., Hourde, C., Duddy, W., Voit, T., Bencze, M., and Dumonceaux, J. (2021). RIPK3-mediated cell death is involved in DUX4-mediated toxicity in facioscapulohumeral dystrophy. J. Cachexia Sarcopenia Muscle *12*, 2079–2090. https://doi.org/10.1002/jcsm.12813.

30. Bosnakovski, D., Choi, S.H., Strasser, J.M., Toso, E.A., Walters, M.A., and Kyba, M. (2014). High-throughput screening identifies inhibitors of DUX4-induced myoblast toxicity. Skelet. Muscle *4*, 4. https://doi.org/10.1186/2044-5040-4-4.

31. An, X., Yu, W., Liu, J., Tang, D., Yang, L., and Chen, X. (2024). Oxidative cell death in cancer: mechanisms and therapeutic opportunities. Cell Death Dis. *15*, 556. https://doi.org/10.1038/s41419-024-06939-5.

32. Heher, P., Ganassi, M., Weidinger, A., Engquist, E.N., Pruller, J., Nguyen, T.H., Tassin, A., Declèves, A.E., Mamchaoui, K., Banerji, C.R.S., et al. (2022). Interplay between mitochondrial reactive oxygen species, oxidative stress and hypoxic adaptation in facioscapulohumeral muscular dystrophy: Metabolic stress as potential therapeutic target. Redox Biol. *51*, 102251. https://doi.org/10.1016/j.redox.2022.102251.

33. Settas, N., Bittel, A.J., and Chen, Y.W. (2025). Increased METTL3 Expression and m6A Methylation in Myoblasts of Facioscapulohumeral Muscular Dystrophy. IJMS *26*, 5170. https://doi.org/10.3390/ijms26115170.

34. Paul, B.T., Manz, D.H., Torti, F.M., and Torti, S.V. (2017). Mitochondria and Iron: current questions. Expert Rev. Hematol. *10*, 65–79. https://doi.org/10.1080/17474086.2016.1268047.

35. Valko, M., Jomova, K., Rhodes, C.J., Kuča, K., and Musílek, K. (2016). Redox- and non-redox-metal-induced formation of free radicals and their role in human disease. Arch. Toxicol. *90*, 1–37. https://doi.org/10.1007/s00204-015-1579-5.

36. Nakamura, K., Ortuste Quiroga, H.P., Horii, N., Fujimaki, S., Moroishi, T., Nakayama, K.I., Hino, S., Saito, Y., Nishino, I., and Ono, Y. (2025). Iron supplementation alleviates pathologies in a mouse model of facioscapulohumeral muscular dystrophy. J. Clin. Investig. *135*, e181881. https://doi.org/10.1172/JCI181881.

37. Balog, J., Thijssen, P.E., Shadle, S., Straasheijm, K.R., van der Vliet, P.J., Krom, Y.D., van den Boogaard, M.L., de Jong, A., F Lemmers, R.J.L., Tawil, R., et al. (2015). Increased DUX4 expression during muscle differentiation correlates with decreased SMCHD1 protein levels at D4Z4. Epigenetics *10*, 1133–1142. https://doi.org/10.1080/15592294.2015.1113798.

38. Jiang, S., Williams, K., Kong, X., Zeng, W., Nguyen, N.V., Ma, X., Tawil, R., Yokomori, K., and Mortazavi, A. (2020). Single-nucleus RNA-seq identifies divergent populations of FSHD2 myotube nuclei. PLoS Genet. *16*, e1008754. https://doi.org/10.1371/journal.pgen.1008754.

39. van den Heuvel, A., Mahfouz, A., Kloet, S.L., Balog, J., van Engelen, B.G.M., Tawil, R., Tapscott, S.J., and van der Maarel, S.M. (2019). Single-cell RNA sequencing in facioscapulohumeral muscular dystrophy disease etiology and development. Hum. Mol. Genet. *28*, 1064–1075. https://doi.org/10.1093/hmg/ddy400.

40. Zheng, D., Wondergem, A., Kloet, S., Willemsen, I., Balog, J., Tapscott, S.J., Mahfouz, A., van den Heuvel, A., and van der Maarel, S.M. (2024). snRNA-seq analysis in multinucleated myogenic FSHD cells identifies heterogeneous FSHD transcriptome signatures associated with

embryonic-like program activation and oxidative stress-induced apoptosis. Hum. Mol. Genet. *33*, 284–298. https://doi.org/10.1093/hmg/ddad186.

41. Yao, Z., Snider, L., Balog, J., Lemmers, R.J.L.F., Van Der Maarel, S.M., Tawil, R., and Tapscott, S.J. (2014). DUX4-induced gene expression is the major molecular signature in FSHD skeletal muscle. Hum. Mol. Genet. *23*, 5342–5352. https://doi.org/10.1093/hmg/ddu251.
42. Rahimov, F., King, O.D., Leung, D.G., Bibat, G.M., Emerson, C.P., Jr., Kunkel, L.M., and Wagner, K.R. (2012). Transcriptional profiling in facioscapulohumeral muscular dystrophy to identify candidate biomarkers. Proc. Natl. Acad. Sci. USA *109*, 16234–16239. https://doi.org/10.1073/pnas.1209508109.
43. Osborne, R.J., Welle, S., Venance, S.L., Thornton, C.A., and Tawil, R. (2007). Expression profile of FSHD supports a link between retinal vasculopathy and muscular dystrophy. Neurology *68*, 569–577. https://doi.org/10.1212/01.wnl.0000251269.31442.d9.
44. Tasca, G., Pescatori, M., Monforte, M., Mirabella, M., Iannaccone, E., Frusciante, R., Cubeddu, T., Laschena, F., Ottaviani, P., and Ricci, E. (2012). Different molecular signatures in magnetic resonance imaging-staged facioscapulohumeral muscular dystrophy muscles. PLoS One *7*, e38779. https://doi.org/10.1371/journal.pone.0038779.
45. Geng, L.N., Yao, Z., Snider, L., Fong, A.P., Cech, J.N., Young, J.M., van der Maarel, S.M., Ruzzo, W.L., Gentleman, R.C., Tawil, R., and Tapscott, S.J. (2012). DUX4 activates germline genes, retroelements, and immune mediators: implications for facioscapulohumeral dystrophy. Dev. Cell *22*, 38–51. https://doi.org/10.1016/j.devcel.2011.11.013.
46. Choi, S.H., Gearhart, M.D., Cui, Z., Bosnakovski, D., Kim, M., Schennum, N., and Kyba, M. (2016). DUX4 recruits p300/CBP through its C-terminus and induces global H3K27 acetylation changes. Nucleic Acids Res. *44*, 5161–5173. https://doi.org/10.1093/nar/gkw141.
47. Chen, W., Zhang, X., Zhang, B., Chi, M., and Zheng, Q. (2025). HRAS Induces Ferroptosis through Upregulating HSPB1 in Hepatocellular Carcinoma. Comb. Chem. High Throughput Screen. *28*, 2502–2510. https://doi.org/10.2174/0113862073306462240710174817.
48. Hayano, M., Yang, W.S., Corn, C.K., Pagano, N.C., and Stockwell, B.R. (2016). Loss of cysteinyl-tRNA synthetase (CARS) induces the transsulfuration pathway and inhibits ferroptosis induced by cystine deprivation. Cell Death Differ. *23*, 270–278. https://doi.org/10.1038/cdd.2015.93.
49. Ou, Y., Wang, S.J., Li, D., Chu, B., and Gu, W. (2016). Activation of SAT1 engages polyamine metabolism with p53-mediated ferroptotic responses. Proc. Natl. Acad. Sci. USA *113*, E6806–E6812. https://doi.org/10.1073/pnas.1607152113.
50. Wu, F., Xiong, G., Chen, Z., Lei, C., Liu, Q., and Bai, Y. (2022). SLC3A2 inhibits ferroptosis in laryngeal carcinoma via mTOR pathway. Hereditas *159*, 6. https://doi.org/10.1186/s41065-022-00225-0.
51. Xie, Y., Zhu, S., Song, X., Sun, X., Fan, Y., Liu, J., Zhong, M., Yuan, H., Zhang, L., Billiar, T.R., et al. (2017). The Tumor Suppressor p53 Limits Ferroptosis by Blocking DPP4 Activity. Cell Rep. *20*, 1692–1704. https://doi.org/10.1016/j.celrep.2017.07.055.
52. Zhang, Y., Shi, J., Liu, X., Feng, L., Gong, Z., Koppula, P., Sirohi, K., Li, X., Wei, Y., Lee, H., et al. (2018). BAP1 links metabolic regulation of ferroptosis to tumour suppression. Nat. Cell Biol. *20*, 1181–1192. https://doi.org/10.1038/s41556-018-0178-0.
53. Chen, X., Comish, P.B., Tang, D., and Kang, R. (2021). Characteristics and Biomarkers of Ferroptosis. Front. Cell Dev. Biol. *9*, 637162. https://doi.org/10.3389/fcell.2021.637162.
54. Yu, Y., Xie, Y., Cao, L., Yang, L., Yang, M., Lotze, M.T., Zeh, H.J., Kang, R., and Tang, D. (2015). The ferroptosis inducer erastin enhances sensitivity of acute myeloid leukemia cells to chemotherapeutic agents. Mol. Cell. Oncol. *2*, e1054549. https://doi.org/10.1080/23723556.2015.1054549.
55. Wong, C.J., Wang, L.H., Friedman, S.D., Shaw, D., Campbell, A.E., Budech, C.B., Lewis, L.M., Lemmers, R.J.F.L., Statland, J.M., van der Maarel, S.M., et al. (2020). Longitudinal measures of RNA expression and disease activity in FSHD muscle biopsies. Hum. Mol. Genet. *29*, 1030–1043. https://doi.org/10.1093/hmg/ddaa031.
56. Bosnakovski, D., Xu, Z., Gang, E.J., Galindo, C.L., Liu, M., Simsek, T., Garner, H.R., Agha-Mohammadi, S., Tassin, A., Coppée, F., et al. (2008). An isogenetic myoblast expression screen identifies DUX4-mediated FSHD-associated molecular pathologies. EMBO J. *27*, 2766–2779. https://doi.org/10.1038/emboj.2008.201.
57. Jones, T.I., Chen, J.C.J., Rahimov, F., Homma, S., Arashiro, P., Beermann, M.L., King, O.D., Miller, J.B., Kunkel, L.M., Emerson, C.P., Jr., et al. (2012). Facioscapulohumeral muscular dystrophy family studies of DUX4 expression: evidence for disease modifiers and a quantitative model of pathogenesis. Hum. Mol. Genet. *21*, 4419–4430. https://doi.org/10.1093/hmg/dds284.
58. Saad, N.Y., Al-Kharsan, M., Garwick-Coppens, S.E., Chermahini, G.A., Harper, M.A., Palo, A., Boudreau, R.L., and Harper, S.Q. (2021). Human miRNA miR-675 inhibits DUX4 expression and may be exploited as a potential treatment for Facioscapulohumeral muscular dystrophy. Nat. Commun. *12*, 7128. https://doi.org/10.1038/s41467-021-27430-1.
59. Mikolajewicz, N., Zimmermann, E.A., Willie, B.M., and Komarova, S.V. (2018). Mechanically stimulated ATP release from murine bone cells is regulated by a balance of injury and repair. eLife *7*, e37812. https://doi.org/10.7554/eLife.37812.
60. Bentzinger, C.F., Wang, Y.X., von Maltzahn, J., Soleimani, V.D., Yin, H., and Rudnicki, M.A. (2013). Fibronectin regulates Wnt7a signaling and satellite cell expansion. Cell Stem Cell *12*, 75–87. https://doi.org/10.1016/j.stem.2012.09.015.
61. Pisconti, A., Bernet, J.D., and Olwin, B.B. (2012). Syndecans in skeletal muscle development, regeneration and homeostasis. Muscles Ligaments Tendons J. *2*, 1–9.
62. Martinvalet, D., Zhu, P., and Lieberman, J. (2005). Granzyme A induces caspase-independent mitochondrial damage, a required first step for apoptosis. Immunity *22*, 355–370. https://doi.org/10.1016/j.immuni.2005.02.004.
63. Dixon, S.J., Lemberg, K.M., Lamprecht, M.R., Skouta, R., Zaitsev, E.M., Gleason, C.E., Patel, D.N., Bauer, A.J., Cantley, A.M., Yang, W.S., et al. (2012). Ferroptosis: an iron-dependent form of nonapoptotic cell death. Cell *149*, 1060–1072. https://doi.org/10.1016/j.cell.2012.03.042.
64. Wang, T., Tomas, D., Perera, N.D., Cuic, B., Luikinga, S., Viden, A., Barton, S.K., McLean, C.A., Samson, A.L., Southon, A., et al. (2022). Ferroptosis mediates selective motor neuron death in amyotrophic lateral sclerosis. Cell Death Differ. *29*, 1187–1198. https://doi.org/10.1038/s41418-021-00910-z.
65. Huang, Y., Wu, B., Shen, D., Chen, J., Yu, Z., and Chen, C. (2021). Ferroptosis in a sarcopenia model of senescence accelerated mouse prone 8 (SAMP8). Int. J. Biol. Sci. *17*, 151–162. https://doi.org/10.7150/ijbs.53126.
66. Bornman, L., Rossouw, H., Gericke, G.S., and Polla, B.S. (1998). Effects of iron deprivation on the pathology and stress protein expression in murine X-linked muscular dystrophy. Biochem. Pharmacol. *56*, 751–757. https://doi.org/10.1016/s0006-2952(98)00055-0.
67. Zhang, Q., Qu, H., Chen, Y., Luo, X., Chen, C., Xiao, B., Ding, X., Zhao, P., Lu, Y., Chen, A.F., and Yu, Y. (2022). Atorvastatin Induces Mitochondria-Dependent Ferroptosis via the Modulation of Nrf2-xCT/GPx4 Axis. Front. Cell Dev. Biol. *10*, 806081. https://doi.org/10.3389/fcell.2022.806081.
68. Corna, G., Caserta, I., Monno, A., Apostoli, P., Manfredi, A.A., Camaschella, C., and Rovere-Querini, P. (2016). The Repair of Skeletal Muscle Requires Iron Recycling through Macrophage Ferroportin. J. Immunol. *197*, 1914–1925. https://doi.org/10.4049/jimmunol.1501417.
69. Ding, H., Chen, S., Pan, X., Dai, X., Pan, G., Li, Z., Mai, X., Tian, Y., Zhang, S., Liu, B., et al. (2021). Transferrin receptor 1 ablation in satellite cells impedes skeletal muscle regeneration through activation of ferroptosis. J. Cachexia Sarcopenia Muscle *12*, 746–768. https://doi.org/10.1002/jcsm.12700.

70. Sorokin, L.M., Morgan, E.H., and Yeoh, G.C. (1987). Transferrin receptor numbers and transferrin and iron uptake in cultured chick muscle cells at different stages of development. J. Cell. Physiol. *131*, 342–353. https://doi.org/10.1002/jcp.1041310306.

71. Matsuda, R. (1987). Regenerating skeletal muscle contains transferrin and a transferrin-dependent growth factor. Biomed. Res. *8*, 133–136. https://doi.org/10.2220/biomedres.8.133.

72. Ikeda, Y., Satoh, A., Horinouchi, Y., Hamano, H., Watanabe, H., Imao, M., Imanishi, M., Zamami, Y., Takechi, K., Izawa-Ishizawa, Y., et al. (2019). Iron accumulation causes impaired myogenesis correlated with MAPK signaling pathway inhibition by oxidative stress. FASEB J. *33*, 9551–9564. https://doi.org/10.1096/fj.201802724RR.

73. Mao, C., Lei, G., Horbath, A., Wang, M., Lu, Z., Yan, Y., Liu, X., Kondiparthi, L., Chen, X., Cheng, J., et al. (2024). Unraveling ETC complex I function in ferroptosis reveals a potential ferroptosis-inducing therapeutic strategy for LKB1-deficient cancers. Mol. Cell *84*, 1964–1979.e6. https://doi.org/10.1016/j.molcel.2024.04.009.

74. Arbogast, S., Kotzur, H., Frank, C., Compagnone, N., Sutra, T., Pillard, F., Pietri, S., Hmada, N., Moussa, D.M.A., Bride, J., et al. (2022). ANT1 overexpression models: Some similarities with facioscapulohumeral muscular dystrophy. Redox Biol. *56*, 102450. https://doi.org/10.1016/j.redox.2022.102450.

75. Arahata, K., Ishihara, T., Fukunaga, H., Orimo, S., Lee, J.H., Goto, K., and Nonaka, I. (1995). Inflammatory response in facioscapulohumeral muscular dystrophy (FSHD): immunocytochemical and genetic analyses. Muscle Nerve. Suppl. *2*, S56–S66.

76. Corasolla Carregari, V., Monforte, M., Di Maio, G., Pieroni, L., Urbani, A., Ricci, E., and Tasca, G. (2020). Proteomics of Muscle Microdialysates Identifies Potential Circulating Biomarkers in Facioscapulohumeral Muscular Dystrophy. Int. J. Mol. Sci. *22*, 290. https://doi.org/10.3390/ijms22010290.

77. Wen, Q., Liu, J., Kang, R., Zhou, B., and Tang, D. (2019). The release and activity of HMGB1 in ferroptosis. Biochem. Biophys. Res. Commun. *510*, 278–283. https://doi.org/10.1016/j.bbrc.2019.01.090.

78. Mobarra, N., Shanaki, M., Ehteram, H., Nasiri, H., Sahmani, M., Saeidi, M., Goudarzi, M., Pourkarim, H., and Azad, M. (2016). A Review on Iron Chelators in Treatment of Iron Overload Syndromes. Int. J. Hematol. Oncol. Stem Cell Res. *10*, 239–247.

79. Alves, F.M., Kysenius, K., Caldow, M.K., Hardee, J.P., Chung, J.D., Trieu, J., Hare, D.J., Crouch, P.J., Ayton, S., Bush, A.I., et al. (2022). Iron overload and impaired iron handling contribute to the dystrophic pathology in models of Duchenne muscular dystrophy. J. Cachexia Sarcopenia Muscle *13*, 1541–1553. https://doi.org/10.1002/jcsm.12950.

80. Chen, G., Ning, B., and Shi, T. (2019). Single-Cell RNA-Seq Technologies and Related Computational Data Analysis. Front. Genet. *10*, 317. https://doi.org/10.3389/fgene.2019.00317.

81. Homma, S., Chen, J.C.J., Rahimov, F., Beermann, M.L., Hanger, K., Bibat, G.M., Wagner, K.R., Kunkel, L.M., Emerson, C.P., Jr., and Miller, J.B. (2012). A unique library of myogenic cells from facioscapulohumeral muscular dystrophy subjects and unaffected relatives: family, disease and cell function. Eur. J. Hum. Genet. *20*, 404–410. https://doi.org/10.1038/ejhg.2011.213.

82. Tirosh, I., Izar, B., Prakadan, S.M., Wadsworth, M.H., 2nd, Treacy, D., Trombetta, J.J., Rotem, A., Rodman, C., Lian, C., Murphy, G., et al. (2016). Dissecting the multicellular ecosystem of metastatic melanoma by single-cell RNA-seq. Science *352*, 189–196. https://doi.org/10.1126/science.aad0501.

83. Banerji, C.R.S., and Zammit, P.S. (2019). PAX7 target gene repression is a superior FSHD biomarker than DUX4 target gene activation, associating with pathological severity and identifying FSHD at the single-cell level. Hum. Mol. Genet. *28*, 2224–2236. https://doi.org/10.1093/hmg/ddz043.

84. Hafemeister, C., and Satija, R. (2019). Normalization and variance stabilization of single-cell RNA-seq data using regularized negative binomial regression. Genome Biol. *20*, 296. https://doi.org/10.1186/s13059-019-1874-1.

85. Schindelin, J., Arganda-Carreras, I., Frise, E., Kaynig, V., Longair, M., Pietzsch, T., Preibisch, S., Rueden, C., Saalfeld, S., Schmid, B., et al. (2012). Fiji: an open-source platform for biological-image analysis. Nat. Methods *9*, 676–682. https://doi.org/10.1038/nmeth.2019.

86. Pandey, S.N., Khawaja, H., and Chen, Y.W. (2015). Culture Conditions Affect Expression of DUX4 in FSHD Myoblasts. Molecules *20*, 8304–8315. https://doi.org/10.3390/molecules20058304.

87. Couto, N.F., Pedersane, D., Rezende, L., Dias, P.P., Corbani, T.L., Bentini, L.C., Oliveira, A.C.S., Kelles, L.F., Castro-Gomes, T., and Andrade, L.O. (2017). LAMP-2 absence interferes with plasma membrane repair and decreases T. cruzi host cell invasion. PLoS Negl. Trop. Dis. *11*, e0005657. https://doi.org/10.1371/journal.pntd.0005657.

88. Hao, Y., Hao, S., Andersen-Nissen, E., Mauck, W.M., 3rd, Zheng, S., Butler, A., Lee, M.J., Wilk, A.J., Darby, C., Zager, M., et al. (2021). Integrated analysis of multimodal single-cell data. Cell *184*, 3573–3587.e29. https://doi.org/10.1016/j.cell.2021.04.048.

89. Becht, E., McInnes, L., Healy, J., Dutertre, C.A., Kwok, I.W.H., Ng, L.G., Ginhoux, F., and Newell, E.W. (2018). Dimensionality reduction for visualizing single-cell data using UMAP. Nat. Biotechnol. *37*, 38–44. https://doi.org/10.1038/nbt.4314.

90. Miller, S.A., Policastro, R.A., Sriramkumar, S., Lai, T., Huntington, T.D., Ladaika, C.A., Kim, D., Hao, C., Zentner, G.E., and O'Hagan, H.M. (2021). LSD1 and Aberrant DNA Methylation Mediate Persistence of Enteroendocrine Progenitors That Support BRAF-Mutant Colorectal Cancer. Cancer Res. *81*, 3791–3805. https://doi.org/10.1158/0008-5472.CAN-20-3562.

91. Krämer, A., Green, J., Pollard, J., and Tugendreich, S. (2014). Causal analysis approaches in Ingenuity Pathway Analysis. Bioinformatics *30*, 523–530. https://doi.org/10.1093/bioinformatics/btt703.

92. Kolberg, L., Raudvere, U., Kuzmin, I., Adler, P., Vilo, J., and Peterson, H. (2023). g:Profiler—interoperable web service for functional enrichment analysis and gene identifier mapping (2023 update). Nucleic Acids Res. *51*, W207–W212. https://doi.org/10.1093/nar/gkad347.

93. DeLong, E.R., DeLong, D.M., and Clarke-Pearson, D.L. (1988). Comparing the areas under two or more correlated receiver operating characteristic curves: a nonparametric approach. Biometrics *44*, 837–845.

STAR★METHODS

KEY RESOURCES TABLE

REAGENT or RESOURCE	SOURCE	IDENTIFIER
Chemicals, peptides, and recombinant proteins		
Gibco DMEM, high glucose, pyruvate	ThermoFisher	Cat# 11995065
Medium 199, Earle's Salts	ThermoFisher	11150067
Fetal Bovine Serum, Premium	Bio-Techne	Cat# S11150
Zinc sulfate heptahydrate (7446-20-0)	Sigma-Aldrich	221376
Hepatocyte Growth Factor Protein, Recombinant human	Sigma-Aldrich	GF116
Human Recombinant bFGF-2, 50ug	Biopioneer	HRP-0011
HEPES (CAS 7365-45-9)	Sigma-Aldrich	Cat# 54457
Dexamathasone (CAS 50-02-2)	Sigma-Aldrich	D4902
Gibco Horse Serum, heat inactivated, New Zealand origin	ThermoFisher	Cat# 26050088
L-Glutamine (200 mM) – 20 mL (CAS 56-85-9)	ThermoFisher	25030149
Antibiotic Antimycotic Solution (100×), Stabilized, 100 mL	Sigma-Aldrich	A5955-100 ML
Gibco Sodium Pyruvate (100 mM)	ThermoFisher	Cat# 11360070
FM1-43 dye ((N-(3-Triethylammoniumpropyl)-4-(4-(Dibutylamino) Styryl) Pyridinium Dibromide)	ThermoFisher	Cat# T3163
Calcium Chloride ($CaCl_2$) (CAS 10043-52-4)	Sigma-Aldrich	Cat# C4901
Hanks Balanced Salts Solution	Sigma-Aldrich	Cat# H9269
Primer-Probe TaqMan Primer Mix	ThermoFisher	Hs07287098_g1
RPL13A Primer-Probe TaqMan Primer Mix	ThermoFisher	Hs04194366_g1
QIAcuity Probe PCR Kit	Qiagen	250102
QIAcuity Nanoplate 26k 24-well	Qiagen	250001
SuperScript™ IV Reverse Transcriptase	Invitrogen	Cat# 18090010
Oligo(dT)12–18 Primer	Invitrogen	Cat# 18418012
SYBR Green Master Mix	Applied Biosystems	Cat# 4309155
GoTaq Green Master Mix	Promega	Cat# M712
100 μM dNTPs	Invitrogen	Cat# 18427013
Gibco PBS, pH 7.4	ThermoFisher	Cat# 10010023
Cell Scraper – UltraCruz®	Santa Cruz Biotechnology	sc-395250
Ammonium iron(II) sulfate hexahydrate (CAS 7783-85-9)	Millipore Sigma	215406
2,2′-Bipyridyl (366-18-7)	Sigma-Aldrich	D216305
Dimethyl sulfoxide (CAS 67-68-5)	Millipore Sigma	472301
Ferrostatin-1 (CAS 347174-05-4)	Sigma Aldrich	SML0583-25 MG
FITC-conjugated Dextran dye (CAS 60842-46-8)	Sigma-Aldrich	FD40S
Propidium Iodide (CAS 25535-16-4)	Invitrogen	P3566
4′,6-diamidino-2-phenylindole (CAS 28718-90-3)	Invitrogen	D1306
Calcein AM green dye (CAS 148504-34-1)	ThermoFisher	C1430
Ultrapure BSA	ThermoFisher	AM2616
FerroOrange	Dojindo Molecular Technologies Inc	F374
BODIPY™ 581/591 C11 undecanoic acid (CAS 217075-36-0)	ThermoFisher	D3861
Trizol Reagent	ThermoFisher	15596026

(*Continued on next page*)

Continued

REAGENT or RESOURCE	SOURCE	IDENTIFIER
Critical commercial assays		
10x Genomics Chromium System	10X Genomics	N/A
Chromium Next GEM Single Cell 3′ GEM, Library & Gel Bead Kit v3.1, 16 rxns	10X Genomics	1000268
Chromium Next GEM Chip G Single cell kit, 16 rxns	10X Genomics	1000127
Deposited data		
Single Cell RNA Sequencing of Injured and Uninjured Myoblasts	NCBI Gene Expression Omnibus (GEO) database	GSE303359
Experimental models: Cell lines		
Immortalized myoblasts	Senator Paul Wellstone Muscular Dystrophy Cooperative Research Center & Dr. Woodring Erik Wright at UT Southwestern University	N/A
Software and algorithms		
Seurat	Hao et al. (2021)[79]	https://satijalab.org/seurat/
SCTransform	Hafemeister et al. (2019)[81]	doi: https://doi.org/10.1186/s13059-019-1874-1
GraphPad Prism v10.3.0	GraphPad	https://www.graphpad.com/
SPSS V30	IBM	https://www.ibm.com/products/spss-statistics
Ingenuity Pathway Analysis	Qiagen	N/A
g:Profiler	Kolberg et al. (2023)[82]	doi: https://doi.org/10.1093/nar/gkad347
GEO2R	GEO Database	https://www.ncbi.nlm.nih.gov/geo/geo2r/
Biomarker_app	Banerji et al. (2019)[83]	doi: https://doi.org/10.1093/hmg/ddz043
Cell Ranger version 6.1.2	10X Genomics	https://www.10xgenomics.com/support/software/cell-ranger/latest
R version 4.1.2	R Project	https://cran.r-project.org/bin/windows/base/old/
scProportionTest	Miller et al. (2021)[84]	doi: https://doi.org/10.1158/0008-5472.CAN-20-3562
ImageJ	Schindelin et al. (2012)[85]	https://imagej.net/ij/

EXPERIMENTAL MODEL AND STUDY PARTICIPANT DETAILS

Myoblasts from four separate individuals with FSHD, and from their healthy, first-degree relatives, were obtained from Dr. Woodring Erik Wright at UT Southwestern University (Texas, USA) and the Senator Paul Wellstone Muscular Dystrophy Cooperative Research Center at Boston Biomedical Research Institute (Boston, MA, USA). The isolation, immortalization, and molecular diagnoses of the myoblasts used in this study were described previously[81] (Table S1). Myoblasts used in this study were derived from male and female, healthy and FSHD donors, as outlined in Table S1. Myoblasts were not tested for mycoplasma. All procedures were carried out in accordance with institutional policies at Children's National Hospital (IACUC no. 00030340, IBC# 21–10051). Sex (male or female) was included in all logistic regression analyses to evaluate the influence of sex on the relationship between Ferroptosis Severity Score and skeletal muscle inflammation.

Cell culture

Culturing conditions were modified from Pandey et al. (2015)[86] as described previously.[22] For all experiments, the cells were weaned from dexamethasone for 3 days by changing to media without dexamethasone (-DEX). For differentiation, FSHD myoblasts were seeded at 80,000 cells/cm^2 in media with dexamthasone. After 24 hrs, myoblasts were transitioned to differentiation media (4:1 DMEM:media 199, 2% horse serum, 2 mM L-glutamine, 1% antibiotics/antimycotics, 1 mM sodium pyruvate, 0.02M HEPES) for 5 days, prior to collection for RNA isolation.

METHOD DETAILS

Cell injury assays

Two cell injury assays were used to determine the effects of plasma membrane rupture. We used a cell scraping approach to induce membrane injuries in thousands of cells simultaneously, as outlined by.[87] Briefly, cells were plated in 10 cm dishes, cultured in -DEX media for 3 days and scraped from the dish with a cell scraper (UltraCruz, Santa Cruz Biotechbology, Dallas, TX). The cells were collected, gently pelleted (130xg, 4 min), resuspended in 1 mL of -DEX media, and re-plated for 6- or 24-hrs for collection for single cell library generation, digital PCR, and RT-PCR. Focused laser membrane ablation assays were performed as previously described.[22] The change in FM1-43 dye fluorescence intensity (ΔF/F0) during the course of the imaging (120 s) was averaged for each condition and plotted. Successful repair was determined by the entry of FM1-43 dye into the cell interior, where a plateau in FM1-43 dye increase indicated successful repair, and failure to repair was indicated by unabated FM1-43 dye increase.

Cell treatments

To increase labile iron, cells were treated for 24 h with 1 mM ferrous ammonium sulfate (FAS, dissolved in water) (FisherScientific, Hampton MA, USA) in -DEX media. To chelate cellular labile iron, cells were treated for 3 h ours with 1 mM 2,2′-Bipyridyl (BPY, dissolved in DMSO, Sigma Aldrich, St. Louis, MO, USA) in cell imaging media (CIM: Hanks Balanced Salts Solution with 10 mM HEPES, 2 mM Ca^{2+}, pH 7.4). To reduce lipid peroxidation, cells were treated with 10 μM Ferrostatin-1 (Selleck Chemicals, Houston, TX, USA) in -DEX media for 24 h prior to laser injury experiments.

Acute cell death assay

To determine the effect of bulk cell injury on FSHD vs. Healthy acute cell death, cells were scraped in the presence of 50 μM cell-impermeant FITC-conjugated Dextran dye (Sigma-Aldrich, FD40S), which accumulates in the cytoplasm of injured cells. Scraped cells were centrifuged (130xg, 4 min) and subsequently resuspended with 3 μM propidium iodide (PI, Invitrogen P3566, Waltham, MA, USA) and 10 μg/ml DAPI (Invitrogen D1306) in CIM for 10 min on ice. PI binds to double stranded DNA but is excluded from cells with intact plasma membranes. Cells were immediately plated in Lab Tek II Chamber Slides (Nunc, Thermo Fisher, Waltham, MA, USA), and imaged on a Leica Thunder imaging system (Leica Microsystems, Wetzlar, Germany). Dextran(+)/PI(−) was used as a marker of cells that were injured and repaired effectively, while Dextran(+)/PI(+) cells denote cells that failed to repair.

Iron chelation assay

To measure the chelation capacity and kinetics of BPY, cells were seeded into 24-well wells in duplicate, cultured in -DEX media for 3 days, washed 3x with 1X PBS, and stained with 2 μM cell-permeant calcein AM green dye (ThermoFisher C1430) and 5 μg/ml DAPI (ThermoFisher 62248) for 15 min. Following baseline incubation, cells were imaged for green fluorescence (496 nm excitation, 516 nm emission) and blue fluorescence (359 nm excitation, 461 nm emission) using a Tecan Spark Plate Reader (Tecan Life Sciences, Männedorf, Switzerland). 1 mM BPY was subsequently added to the CIM, and images were taken at 60-min intervals over the next 180 min. Calcein fluorescence intensity was normalized to DAPI intensity to control for cell density.

Single cell transcriptomics platform: 10x chromium

FSHD myoblasts from donors 1 and 2, and myoblasts from their healthy siblings (healthy 1 and healthy 2) cultured above were cultured for 3 days in -DEX media (as described above) and subjected to scrape injury assays as described above. Cells were collected at 6- and 24-hrs post-injury, centrifuged for 4 min at 800 rpm (130xg) at room temperature, washed once with 1X PBS, and resuspended in in 1X PBS supplemented with 0.04% ultrapure BSA (ThermoFisher Scientific). The 10x Genomics Chromium System (10x Genomics Inc, San Francisco, CA, USA) was used for single cell library generation following the instructions in the Chromium Single Cell 3' Gel Bead-in-Emulsion (GEM), Library & Gel Bead Kit v3 (10x Genomics). The number of cells loaded on the system was calculated based on the desired number of captured cells (8,000 cells/sample) following manufacturer's instructions.

scRNA-sequencing and processing of 10x genomics chromium scRNA-seq data

Each scRNA-seq library was pair-end sequenced in a single cell flow lane on an Illumina HiSeq (Illumina, San Deigo, CA) using the S1 flow cell (targeting 50,000 reads/cell). Sequencing reads were processed with the Cell Ranger version 6.1.2 (10X Genomics) and aligned to the human reference genome GRCh38 – hg38. Sequencing information can be found in Table S2. From the gene expression matrix, the downstream analysis was carried out with R version 4.1.2. Quality control, filtering, data clustering and visualization, and the differential expression analysis was carried out using Seurat version 4.3.2 R package.[88] For each individual dataset, cells <200 UMIs and <200 genes were removed from the gene expression matrix. In addition, we removed any single-cell with >15% UMIs mapped to mitochondrial genes, as well as obvious outliers in number of UMIs (cell doublets). Data were normalized by SCTransform normalization from Seurat.[84] We performed principal component analysis on the gene expression matrix and used the first 15 principal components for clustering and visualization. Unsupervised shared nearest neighbor (SNN) clustering was performed with a resolution of 0.5 and visualization was done using uniform manifold approximation and projection (UMAP).[89]

At each timepoint (baseline, 6-hrs) FSHD and Healthy samples were integrated using the Seurat Integrate Layers Function. From the integrated object, Seurat's "FindConservedMarkers" was used to identify differentially expressed genes shared between FSHD

and Healthy myocytes in each cluster compared to all other clusters. The ''FindAllMarkers'' function was used to identify differentially expressed genes between FSHD and Healthy myocytes within each cluster. For both analyses, DE genes were defined using a likelihood ratio test that assumes the data follows a negative binomial distribution and only considering genes with > log2(0.25) fold-change and expressed in at least 25% of cells in the cluster. Additionally, at each timepoint, we performed a ''pseudobulk'' DE analysis using Seurat's ''AggregateExpression'' function to sum together gene counts of all the cells from the same sample (baseline, 6-h) for each cell type (FSHD or Healthy). This results in one gene expression profile per sample and cell type. We can then perform DE analysis using DESeq2 on the sample level. This treats the samples, rather than the individual cells, as independent observations. The Seurat function ''AddModuleScore'' was used to evaluate the expression characteristics of marker gene sets, as previously described.[82] Finally, testing for significant changes in cluster composition regarding the contribution of FSHD vs. Healthy myoblasts at each integrated timepoint was performed using the scProportionTest package.[90]

Functional annotations

Ingenuity Pathway Analysis (IPA, Qiagen GmbH, Hilden, Germany) was used identify enriched cell signaling pathways (canonical pathways) among DEG in our dataset (p-value calculated using the right-tailed Fisher's Exact Test). Predicted Activation or inhibition of canonical pathways were expressed in z-scores, as calculated in Krämer et al. (2014).[91] The Benjamini-Hochberg (B-H) method was used to control for multiple comparisons. Gene Ontology analysis of DE genes was performed using g:Profiler[92] at a threshold of $p < 0.05$.

Live cell imaging

Live cell immunofluorescence was used to quantify cytosolic labile iron using FerroOrange (Dojindo Molecular Technologies Inc, Rockville, MD, USA) – a small molecular iron sensing dye containing a fluorescent probe that selectively binds iron ions. Cells were seeded on glass coverslips, cultured in -DEX media for 3 days, and washed 3x with PBS to thoroughly remove all FBS-containing media. After washing, wells were incubated for 30 min with 1 μM FerroOrange in CIM, washed once with 1X PBS, and imaged using a Leica Thunder imaging system at 20X. To measure lipid peroxidation, cells were seeded on glass coverslips, cultured in -DEX media for 3 days, washed 3x with PBS, and then incubated with 10 μM of BODIPY 581/591 C11 undecanoic acid (ThermoFisher). Oxidation of the polyunsaturated butadienyl portion of BODIPY 581/591 C11 in live cells results in a shift of the fluorescence emission peak from red (~590 nm) to green (~510 nm), allowing ratiometric analysis of lipid peroxidation. The ratio of green fluorescence to (red + green) fluorescence was used to quantify the relative levels of lipid peroxidation. All images were exported as 16-bit tiffs and analyzed in Fiji[85] using standard functions. Background correction as achieved using the built-in ''rolling ball'' algorithm.

RNA isolation, RT-PCR, digital PCR

Total RNA was purified by adding Trizol reagent directly to the cells after being washed twice in PBS, in accordance with the manufacturer's instructions (Invitrogen). RNA was isolated as previously described[22] The primer sequences for *ZSCAN4* was: F – 5′GTGGCCACTGCAATGACAA3′, R – 5′AGCTTCCTGTCCCTGCATGT3′, and *MBD3L2* was: F – 5′CGTTCACCTCTTTTCCAAGC3′, R – 5′AGTCTCATGGGGAGAGCAGA3'. Relative gene expression was analyzed using the delta delta ct method. Digital PCR (dPCR) for DUX4 expression was performed as previously described[33] using 800 ng of undiluted cDNA and the *DUX4* Primer-Probe TaqMan Primer Mix (ThemroFisher, ID: Hs07287098_g1), and *RPL13A* Primer-Probe TaqMan Primer Mix (ThemroFisher ID: ID: Hs04194366_g1). Copies/ul of *DUX4* was normalized to the copies/ul of *RPL13A* for each sample.

Published gene expression data and calculation of ferroptosis severity score

Raw read counts from publicly available microarray and RNA sequencing studies of human FSHD and Healthy muscle biopsies were obtained from Yao et al. (2014) (GSE56787)[41]; Rahimov et al. (2012) (GSE36398)[42]; Dixit et al. (2007) (GSE9397)[3]; Wang et al. (2019) (GSE115650)[15]; Osborne et al. (2007) (GSE10760) [43]; and Tasca et al. (2012) (GSE26852).[44] Median-normalized and log-transformed counts were obtained from GEO database and GEO2R. Microarray data was normalized between arrays for consistency. To enable comparison across datasets, probes in each microarray dataset and sequences in the RNA-seq data were matched to unique gene identifiers (EntrezGene). Probes or sequences mapping to the same gene identifier were averaged. The Ferroptosis Severity Score was calculated as the average expression of markers known to be upregulated during ferroptosis, including prostaglandin-endoperoxide synthase 2 *(PTGS2),* NFE2 like BZIP transcription factor 2 *(NFE2L2),* solute carrier family 40 member 1 *(SLC40A1),* solute carrier family 7 member 11 *(SLC7A11),* aldo-keto reductase family 1 member C1 *(AKR1C1),* ferritin heavy chain 1 *(FTH1),* Thioredoxin Reductase 1 *(TXNRD1),* ChaC glutathione specific gamma *(CHAC1),* ATP binding cassette subfamily C member 1 *(ABCC1),* metallothionein 1G *(MT1G),* NAD(P)H quinone dehydrogenase 1 *(NQO1),* cystathionine beta-synthase *(CBS),* and heme oxygenase-1 *(HMOX1)*.[53]

QUANTIFICATION AND STATISTICAL ANALYSIS

Meta-analysis to assess the discriminatory powers of baseline and 6-hr signature genes, as well as the Ferroptosis Severity Score across muscle biopsy datasets was performed using an inverse variance, random effects model to combine statistics across studies.

The standard mean differences were pooled across studies used to determine the overall difference in expression of each gene signature between FSHD and Healthy muscle biopsies. P-values denoting the significance of the scores for each study were calculated using the Wilcoxon Rank-Sum test. ROC curve analysis was performed using Prism to determine if gene signatures could effectively classify FSHD from Healthy biopsies. The performance of the signatures in binary classification of biopsies as FSHD or Healthy was evaluated using the area under the curve (AUC) and a Mann-Whitney U Test. The performance of each signature in each study was compared using the z-statistic from DeLong's test.[93] Values of the PAX7 target gene repression biomarker and each of the three DUX4 target gene expression biomarkers (Choi et al. 2016, Geng et al. 2012, Yao et al. 2014)[41,45,46] were calculated using the R package developed by Banerji et al. (2019).[83]

A binomial logistic regression was used to determine the predictive ability of sex (male or female), age, repeat length, and Ferroptosis Severity Score on skeletal muscle inflammation (dichotomized to presence or absence) in FSHD muscle biopsies derived from Wang et al. (2019).[15] Overall regression model fit was assessed using the Hosmer-Lemeshow Goodness-of-Fit Test, and the potency of the model was determined using Nagelkerke's Pseudo R^2. Likewise, a Spearman Rank Order Correlation was used to investigate the association between Ferroptosis Severity Score and measures of fat deposition (T1 score), and an additional measure of muscle inflammation (STIR score) (see Wang et al. (2019)[15]). All analyses were performed in SPSS V30 (IBM, Armonk, NY, USA) and Graphpad Prism v10.3.0. (Dotmatics, Boston, MA, USA).

Paired t-tests were used to determine differences between groups for the percentage of cells that failed to repair. Two-way ANOVAs were used to determine the effect of genotype (FSHD vs. Healthy) and time for DUX4 expression, MBD3L2 expression, and ZSCAN4 expression, assessment of aggregate enrichment of biomarkers over time, ferroOrange intensity, calcein kinetics, and oxidized BODIPY. Two-way ANOVAs were also used to investigate the effects of genotype and treatment on ferroOrange intensity following FAS treatment, oxidized BODIPY following FAS treatment, the percentage of cells that failed to repair with FAS treatment, and ferroOrange intensity following BPY treatment. A two-way repeated-measures ANOVA was used to evaluate membrane repair kinetics following BPY and Fer-1 treatments, as well as the percentage of cells that failed to repair following BPY treatment. The exact sample size for all experiments, and the statistical tests used, are listed in the figure legends.